IDENTIFYING GENES IN PANCREATIC BETA-CELL FUNCTION USING A NOVEL HIGH-THROUGHPUT CELL-BASED SCREENING ASSAY

By

FEYZA NUR TUNCER

A Thesis Submitted to the Graduate Faculty of

WAKE FOREST UNIVERSITY GRADUATE SCHOOL OF ARTS AND SCIENCES

In Partial Fulfillment of the Requirements

For the Degree of

Master of Science

In the Molecular Genetics and Genomics Program

December 2008

Winston-Salem, North Carolina

Approved by:

Dr. Peter A. Antinozzi, Ph.D., Advisor _____

Examining Committee:

Dr. E. Ann Tallant, Ph.D., Chairperson _____

Dr. Donald W. Bowden, Ph.D. _____

Dr. Yuh-Hwa Wang, Ph.D. _____

Dr. Bingzhong Xue, Ph.D. _____

ACKNOWLEDGMENTS

I would like to acknowledge my advisor Dr. Peter A. Antinozzi for his teachings; without them this work would be far from complete.

I would also like to thank my committee members for their guidance and direction with my thesis. I would especially like to thank Dr. E. Ann Tallant for her unconditional assistance and support throughout the development of my thesis. It was an honor to have her as my committee chair.

It was also a privilege to collaborate with Dr. Donald W. Bowden and be a part of his group meetings. Dr. Bowden has set an example of an outstanding scientist and that his work ethics will always guide me in my professional life. I appreciate the kindness and the support of all the members of the Bowden lab. In this respect, I would specifically like to thank Dr. Nichole Palmer Allred for her invaluable inputs into my thesis.

I am thankful to Dr. Yuh-Hwa Wang, her lab and Dr. Xue for their help along the way.

I would also like to thank our program's director Dr. Mark Lively for having his doors open whenever I needed a consultation. It was a pleasure to be a part of Molecular Genetics Program that values its students.

I would like to thank my friends for the love and support they provided me with. I would especially like to acknowledge Omur Kayikci, Nadine Shaban and Bhavani Krishnan; without them, I would not be able to make it in Winston-Salem.

I am fortunate to have a wonderful family, who supports and encourages me in every step of my life. Therefore, I dedicate my thesis to my beloved parents Gulistan and Erman Tuncer, for I would not be where I am today without their unconditional love, trust and support in the decisions I make.

TABLE OF CONTENTS

LIST OF TABLES AND FIGURES

LIST OF ABBREVIATIONS

ADP	Adenosine 5'-diphosphate
AIR	Acute insulin response
ANOVA	Analysis of variance
APC	Adenomatous polyposis coli
ATP	Adenosine 5'-triphosphate
bp	Base pair
C.elegans	*Caernorhabditis elegans*
CamKII	Calcium calmodulin-dependent protein kinase II
cDNA	Complementary DNA
CL	Citrate lyase
C-peptide	Connecting peptide
C_t	Threshold cycle
CYCA	*Cyclophilin A*
dbSNP	Single nucleotide polymorphisms database
DI	Disposition index
Dkk	Dickkopf
DMEM	Dulbecco's Modified Eagle Medium
DMRIE-C	1-2-dimyristyloxypropyl-3-dimethyl-hydroxy ethyl ammonium bromide and cholesterol
dNTP	Deoxyribonucleotide triphosphate
dsDNA	Double stranded DNA
Dvl	Disheveled

ELISA	Enzyme-Linked ImmunoSorbent Assay
FBS	Fetal Bovine Serum
FSIGT	Frequently sampled intravenous glucose tolerance test
Fzd	Frizzled
G-protein	GTP binding protein
GSIS	Glucose-stimulated insulin secretion
GSK3β	Glycogen synthase kinase 3beta
GTP	Guanosine 5'-triphosphate
ICDc	Isocitrate dehydrogenase
IFN	Interferon
IRASFS	Insulin Resistance Atherosclerosis Family Study
IRP	Intracellular reserve pool
JNK	c-Jun N-terminal kinase
K^+_{ATP} channel	ATP-sensitive potassium channel
LEF/TCF	Lymphoid enhancer factor/T cell factor
LRP5/6	Low density lipoprotein related protein 5 or 6
MAPK	Mitogen activated protein kinase
MDP	Morphologically docked pool
miRNA	microRNA
mRNA	Messenger RNA
NIDDM	Non-insulin dependent diabetes mellitus
ntRFP	Nuclear targeted red fluorescent protein
PBS	Phosphate-buffered saline

PC	Pyruvate carboxylase
PCP	Planar cell polarity
PDH	Pyruvate dehydrogenase
PKC	Protein kinase C
PMA	Phorbol ester
QPDT	Quantitative Pedigree Disequilibrium Test
qRT-PCR	Quantitative real time-polymerase chain reaction
QTL	Quantitative trait loci
RER	Rough endoplasmic reticulum
Rho-kinase	Rho-associated kinase
RISC	RNA-induced silencing complex
RPMI	Roswell Park Memorial Institute
RRP	Readily releasable pool
SAP	Secretory granule targeted alkaline phosphatase
SEAP	Secreted alkaline phosphatase
sFRP1	Secreted Frizzled related protein 1
shRNA	Short-hairpin RNA
S_I	Insulin sensitivity
siRNA	Small interfering RNA
SNP	Single nucleotide polymorphism
SOLAR	Sequential Oligogenic Linkage Analysis
T2DM	Type 2 diabetes mellitus
TCA	Tricarboxylic acid

T_m	Melting temperature
WRE	Wnt response elements
$[Ca^{2+}]_i$	Intracellular calcium concentration
7TMR	7 transmembrane receptor

Feyza Nur Tuncer

IDENTIFYING GENES IN PANCREATIC BETA-CELL FUNCTION USING A NOVEL HIGH-THROUGHPUT CELL-BASED SCREENING ASSAY

Thesis under direction of Peter A. Antinozzi, Ph.D., Assistant Professor of Biochemistry

ABSTRACT

Type 2 diabetes mellitus is a complex disorder caused by elevated blood glucose levels that arise from peripheral insulin resistance and/or impaired insulin secretion from the pancreatic beta-cells. It is a global epidemic affecting millions of people around the world, bringing serious economic burden to health care systems. Thus, the underlying components of this disorder are under extensive investigation. The interest of my thesis project has been on the insulin secretion phenotype of type 2 diabetes. Therefore, a high-throughput surrogate cell-based assay for pancreatic beta-cell insulin secretion has been developed through which the screen of novel genes and the genes having genetic evidences of susceptibility to type 2 diabetes were screened, in order to assign them pertinent roles in beta-cell secretory function. In this respect, we have screened the Insulin Resistance Atherosclerosis Family Study (IRASFS) positional candidate genes and the Wnt signaling pathway components, where the genes with significant impacts on glucose-stimulated secretion were subject to further delineation. The IRASFS gene list was established through linkage analysis of quantitative trait loci for measures of glucose homeostasis by our collaborator. Our aim was to add a functional layer to the genetic evidence through the screens performed on IRASFS genes. On the other hand, previous reports have shown the involvement of several Wnt signaling pathway components in beta-cell secretory function. In this respect, the strongest evidence comes from

independent genomic studies that have highly associated the development of type 2 diabetes and impaired insulin secretion to the polymorphisms within the *TCF7L2* gene. In addition, an active Wnt signaling pathway was suggested in the mouse and human pancreas by the confirmed expressions of several Wnt and Frizzled isoforms, along with the evidence highlighting the requirement of the co-receptor *LRP5* for glucose-stimulated insulin secretion (GSIS) in the mouse islets. We have performed a general screen on the Wnt signaling pathway components in order to complete the picture between the genes *TCF7L2* and *LRP5* and to delineate this pathway with respect to beta-cell secretory function. Our findings have validated the importance of this pathway, where a β-catenin dependent path of glucose-induced insulin secretion is suggested.

INTRODUCTION

Type 2 diabetes mellitus (T2DM), also referred to as adult-onset diabetes or non-insulin dependent diabetes mellitus (NIDDM), is a metabolic disorder that constitutes more than 90% of the diabetes cases around the world (Kasuga, 2006). It is now estimated that approximately 171 million people are affected by this disorder (Kasuga, 2006), accounting for 6% of the world population (Meetoo et al., 2007) . It is estimated that 336 million people will be diagnosed with type 2 diabetes by the end of 2030 (Kasuga, 2006). T2DM causes serious medical complications including nephropathy, retinopathy, atherosclerosis and stroke, accounting for approximately of 2.9 million deaths per year (WHO, 2006). The medical care costs for T2DM, as well as its complications, challenge the world's health care systems with a serious economic burden. The worldwide cost of this disorder is estimated to be around 213 billion US dollars in 2025 (Allgot B. et al., 2003).

T2DM is characterized by elevated blood glucose levels due to certain phenotypes including peripheral insulin resistance and impaired insulin secretion from the pancreatic beta-cells. The sequence of events prior to diagnosis of this disease would be the induction of insulin resistance, leading to increased insulin biosynthesis and its enhanced secretion from the beta-cells in order to maintain normoglycemia (Prentki and Nolan, 2006). However, type 2 diabetes occurs when insulin secretion from pancreatic beta-cells can no longer compensate for this resistance. A typical prognosis for this disease would be the exhaustion of the beta-cells, leading to an eventual beta-cell dysfunction.

Pancreatic beta-cell function:

Pancreatic beta-cells are the sites of insulin biosynthesis and secretion in response to glucose and other nutrients with the crucial role of adjusting secretion parallel to glucose concentrations. Insulin biosynthesis begins with the translation of preproinsulin messenger RNA (mRNA) that consists of a signal sequence residing on its N-terminal, followed by B chain, which is connected to A chain on the carboxy-terminus via a connecting peptide (C-peptide) sequence (Molina P.E., 2006). The signal sequence directs the insertion of the precursor mRNA into the rough endoplasmic reticulum (RER) during its translation, where the subsequent cleavage of the signal peptide takes place, generating proinsulin (Dodson and Steiner, 1998). Proinsulin folds into its three-dimensional structure within the RER, setting its destination to the Golgi complex. The Golgi sorts proinsulin and the prohormone-converting enzymes into clathrin-coated vesicles, forming the immature secretory vesicles. The vesicles mature as they loose their clathrin-coats and as C-peptide is cleaved from proinsulin through the action of the enzymes with which it resides. As a result, mature uncoated secretory granules contain equimolar amounts of free C-peptide and insulin consisting of A and B chains that are held together by two disulfide bridges (Masharani U. and German M.S., 2007). Hence, the beta-cells secrete insulin and C-peptide in response to elevated glucose concentrations. Figure 1 depicts a diagram of insulin structure and summarizes the path it follows prior to secretion.

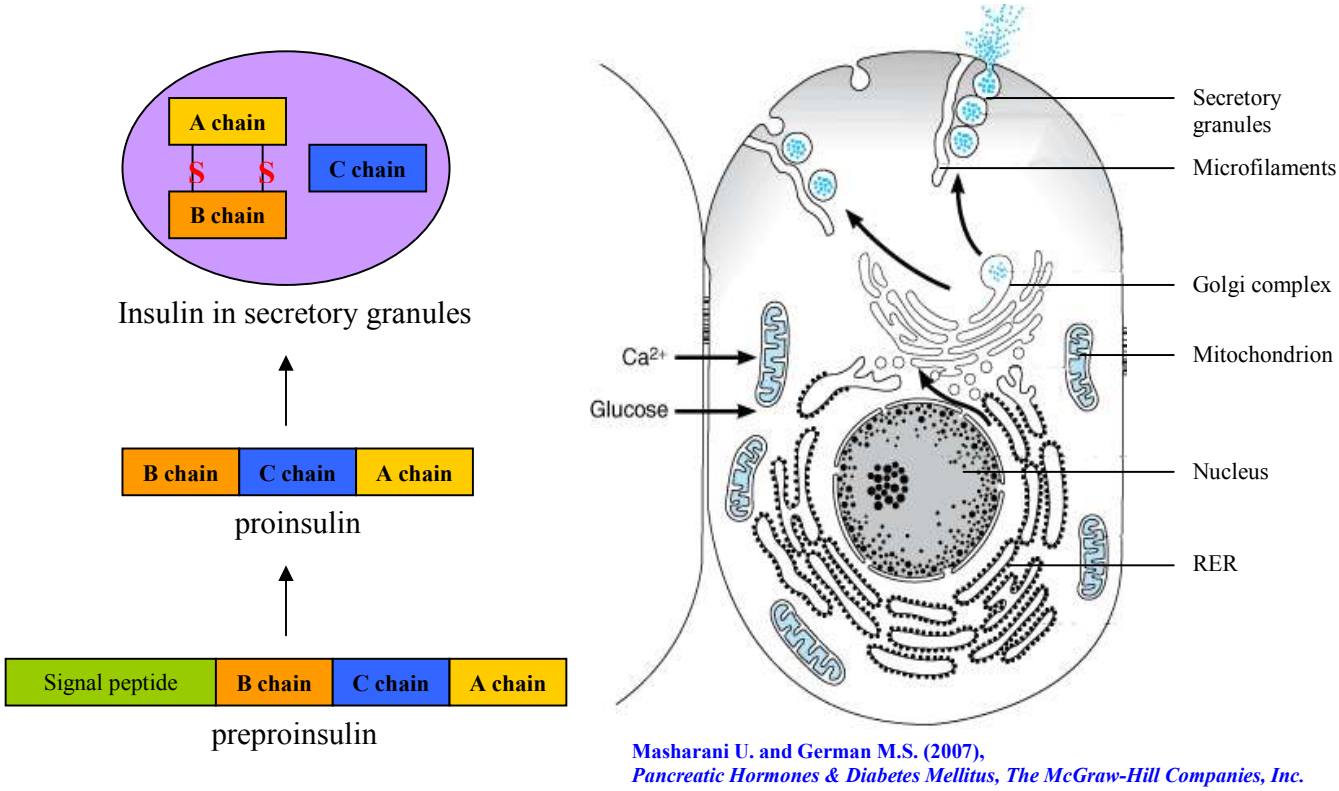

Figure 1. Insulin biosynthesis and its secretion from pancreatic beta-cells. Insulin is synthesized in the nucleus as the precursor mRNA, preproinsulin, that is comprised of a signal peptide on its N-terminal, in addition to B, C and A chains. Directed by the signal peptide, the precursor molecule is translated in the RER, where the signal peptide is cleaved producing proinsulin. Proinsulin is transferred to the Golgi complex to be packaged into clathrin-coated vesicles containing prohormone-converting enzymes. These enzymes cleave the C chain (C-peptide) creating equimolar amounts of free C-peptide, and the insulin hormone formed by A and B chains that are linked by two disulfide bridges depicted as "S" in red color.

Insulin secretion from the pancreatic beta-cells occurs through exocytosis of secretory vesicles in two phases: an acute phase of insulin secretion in the first 10 minutes of glucose stimulation, followed by a sustained phase of insulin secretion corresponding to prolonged glucose stimulation (Muoio and Newgard, 2008). In pancreatic beta-cells, the secretory vesicles reside in different functional pools composed of an intracellular reserve pool (IRP), a morphologically docked pool (MDP) and a readily releasable pool (RRP) that accounts for approximately 90%, 10% and <1% of the beta-cell secretory granules, respectively (MacDonal et al., 2005). The vesicles in the RRP are primed to be released immediately in response to the stimuli and hence are

found to be in close proximity to the voltage-gated Ca^{2+} channels, where an initial influx of calcium would induce exocytosis of these vesicles, forming the acute phase of insulin secretion (MacDonald and Rorsman, 2007). SNARE proteins that are known to mediate the fusion of exocytotic secretory vesicles to the cell membrane are also found to interact with voltage-gated Ca^{2+} channels, coupling calcium influx to the exocytosis of the primed vesicles (Catterall, 1999) (Barg et al., 2002). On the other hand, the sustained phase of insulin secretion in response to prolonged stimuli is established through the exocytosis of mobilized and primed secretory vesicles from the IRP and MDP that replenish the RRP of the secretory vesicles (Rorsman et al., 2000). In this respect, adenosine 5'-triphosphate (ATP) production is essential in vesicle movement along the microtubules within the cytoplasm (Varadi et al., 2002), in addition to its crucial role in vesicle priming, which is characterized as chemical modifications on secretory vesicles required to make them compatible for release (Eliasson et al., 1997). Thus, beta-cell metabolism plays a fundamental role in insulin secretion.

The insulin secretory mechanism itself however depends on the utilization of glucose upon its entry into the beta-cells via facilitated diffusion through the glucose transporter GLUT-2, followed by its subsequent phosphorylation by glucokinase, marking the rate limiting reaction in glucose metabolism (Ashcroft, 2006). Phosphorylated glucose is metabolized by glycolysis generating pyruvate that enters into the tricarboxylic acid (TCA) cycle in equal proportions through the oxidative or the anaplerotic pathways, initiating the mitochondrial metabolism (Muoio and Newgard, 2008) (Figure 2). Reducing equivalents NADH and $FADH_2$ are generated by TCA cycle and are used to deliver electrons to the respiratory chain (electron transport chain), where

transfer of each electron is accompanied by the pumping of a hydrogen ion into the mitochondrial intermembrane space, creating a strong proton electrochemical gradient across the inner mitochondrial membrane. This gradient is used to drive ATP synthesis by the ATP synthase embedded in the mitochondrial membrane (Nelson D.L.and Cox M.M., 2005). Generation of ATP leads to an increase in ATP:Adenosine 5'-diphosphate (ADP) ratio in the cytoplasm. This causes the closure of ATP-sensitive potassium channels (K^+_{ATP} channels), depolarizing the beta-cell membrane that in turn opens voltage-gated calcium channels, increasing intracellular calcium concentration ($[Ca^{2+}]_i$). As a result, exocytosis of the primed secretory vesicles is stimulated in response to the acute phase of insulin secretion (MacDonald and Rorsman, 2007). The sustained phase of insulin secretion is achieved through the role of initial calcium influx in inducing further calcium release from the intracellular stores in response to prolonged glucose stimulation (MacDonald et al., 2005). In such a case, mitochondria take up calcium that is thought to provide sustained ATP generation through activating NADH generating dehydrogenases (Newsholme et al., 2007) and/or through stimulating ATP synthase by dissociating its inhibitor (Wiederkehr and Wollheim, 2006) (MacDonald et al., 2005). This increased ATP:ADP ratio establishes insulin secretion by helping to replenish the RRP of secretory vesicles as described previously. In addition, the K^+_{ATP} channel-independent glucose-stimulated insulin secretion (GSIS) pathway, referred to as the amplification pathway (Henquin, 2000), is thought to contribute to the sustained phase of insulin secretion by producing TCA cycle intermediates to "amplify" the Ca^{2+}-dependent insulin secretion (Newsholme et al., 2007) (Figure 2).

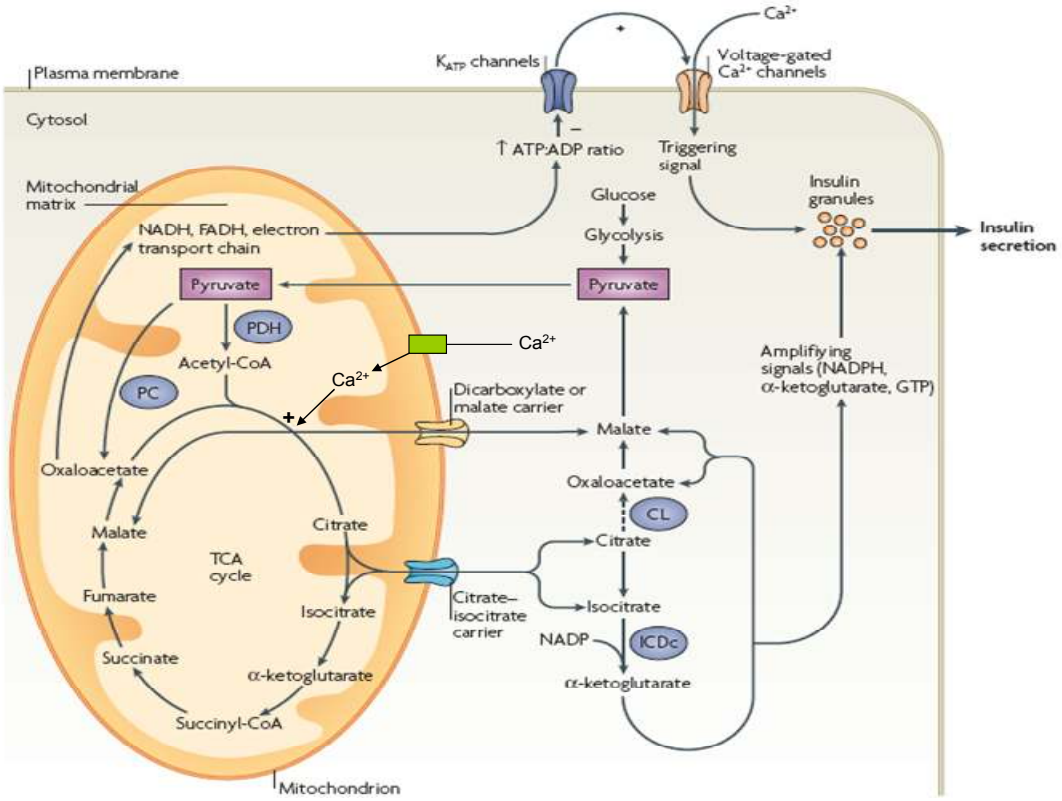

Muioi D.M. and Newgard C.B. (2008), *Molecular and metabolic mechanisms of insulin resistance and β-cell failure in type 2 diabetes, Nature Reviews 9.*

Figure 2. Glucose metabolism and glucose-stimulated insulin secretion (GSIS) in pancreatic beta-cells. Within the beta-cells, glucose is metabolized by glycolysis forming pyruvate. Pyruvate is incorporated into the TCA cycle either through the oxidative pathway (pyruvate dehydrogenase (PDH)) or through the anaplerotic pathway (pyruvate carboxylase (PC)). Reducing agents (NADH, $FADH_2$) produced by the TCA cycle enter into the electron transport chain generating ATP, with the outcome of increased $[Ca^{2+}]_i$ that stimulates exocytosis. Transport of malate and citrate or isocitrate through malate and citrate-isocitrate carriers respectively, contribute to the generation of the amplifying signals comprised of the intermediates formed by interconversion of these components. (CL: citrate lyase, ICDc: isocitrate dehydrogenase)

Several physiological potentiators have been described to augment GSIS, which exert their effects independent of the mitochondrial metabolism. Such a potentiation effect was observed by phorbol ester (PMA) that was shown to activate protein kinase C (PKC) and enhance insulin release without essential changes in the average calcium concentrations (Rutter et al., 2006) (Zaitsev et al., 1995). Activation of PKC is thought to play a role in vesicle priming and thus in replenishing the RRP of secretory vesicles in

the beta-cells (MacDonald et al., 2005). Several studies observed the translocation of PKC isoforms to the beta-cell membrane upon PMA stimulation, where the specific isoform PKC-ε was found to colocalize with the insulin secretory granules, highlighting a strong role for PKC in insulin exocytosis (Zaitsev et al., 1995) (Mendez et al., 2003).

Small interfering RNA (siRNA):

Small interfering RNAs (siRNAs) are double stranded RNAs that are involved in sequence specific, post-transcriptional gene regulation. Due to their specificity in rapid knock-down of gene expression, they have been the choice of high-throughput functional genomic analysis in mammalian cells (DasGupta et al., 2005). siRNAs have also been widely used in the discovery of novel genes, identification of drug targets and in the development of more specific therapeutics (Jackson et al., 2003). In mammalian cells, the endogenous RNA interference pathway is an integral part of the gene expression mechanism that is initiated by the synthesis of double stranded short-hairpin RNAs (shRNAs) from non-coding microRNAs (miRNAs) (Goldman, 2004). In this pathway, shRNAs are processed by RNase III-like enzyme Dicer to produce 20-25 nucleotide long double stranded siRNAs, which unwind upon interaction with RNA-induced silencing complexes (RISCs) that recruit the guide strand (i.e. the single stranded siRNA) to its complimentary sequence in the cognate mRNA (Birmingham et al., 2007). This hybridization targets the mRNA for its cleavage, followed by its subsequent degradation, leading to the loss of *de novo* protein synthesis. In functional genomic studies, synthetically designed siRNAs are transfected into cells to take advantage of this endogenous RNA interference pathway, in which they enter at the level of RISC loading and hence provide a robust gene silencing that was shown to reach maximal effectiveness

generally around 24 hours post-transfection, depending on the cell type (Jackson et al., 2006).

Several studies have reported unintended consequences caused by synthetic siRNA introduction into the mammalian cells. Depending on the cell type, two mechanisms of unintended gene modulations have been proposed: RNA interference independent or RNA interference mediated modulations. The former mechanism consists of siRNAs exceeding 23 base pairs (bp) in length, in addition to siRNAs with particular sequence motifs that can induce innate immune response by activating the interferon (IFN) response pathway (Reynolds et al., 2006). On the other hand, the majority of RNA interference mediated unintended gene modulations occurs as a result of the sequence similarity between the siRNA duplex and a non-targeted mRNA molecule, referred to as off-targeted gene silencing. The primary determinant for such hybridization was linked to the seed sequence of the siRNA duplex, formed by 7 nucleotides on the 5' region of the siRNA guide strand (Jackson et al., 2006). In an attempt to eliminate such side-effects of synthetic siRNAs and to confirm the observed phenotypic outcome from a specific gene knock-down, the use of at least two non-overlapping siRNAs having similar effectiveness in knocking down the expression of the same gene is recommended in high-throughput genetic screens (Echeverri et al., 2006).

A surrogate assay for pancreatic beta-cell insulin secretion has been established in our laboratory by taking advantage of the pancreatic beta-cell secretory mechanism, where siRNA-mediated gene silencing is used in prioritizing genes involved in secretory function. The utilization of this assay formed our approach for the screen of novel genes, as well as the screen of the genes having genetic evidence of susceptibility to T2DM

determined through whole genome association and linkage analysis studies, in an attempt to identify their roles in beta-cell secretory function. In this respect, my thesis is composed of two distinct sets of genetic screens performed through the developed surrogate cell-based assay. These screens were performed on the Wnt signaling pathway components that have an emerging interest with role to impaired insulin secretion, and on the genes from the Insulin Resistance Atherosclerosis Family Study (IRASFS), as a part of our collaborative work with Dr. Donald W. Bowden's laboratory.

The Wnt Signaling Pathway:

Wnt signaling is involved in the regulation of multiple cellular processes such as proliferation, cell motility, cell-fate determination, and establishment of primary axis in vertebrate development (Habas and Dawid, 2005). The components of the Wnt pathway are found to be highly conserved among species including *Caernorhabditis elegans* (*C.elegans)*, *Drosophila*, *Xenopus*, zebra fish, rodents and humans (Kohn and Moon, 2005). The Wnt signaling pathway is subdivided into three different signaling cascades referred to as the "Canonical Pathway", "Planar Cell Polarity (PCP) Pathway" and "Wnt/Ca^{2+} Pathway". All three pathways are activated through the binding of a family of secreted glycoproteins, Wnt ligands, to the cysteine rich domains of seven-transmembrane receptors, Frizzleds (Fzds), which are situated on the cell membrane. Upon this interaction, the cytosolic phosphoprotein Disheveled (Dvl) is phosphorylated and recruited to interact with the cytosolic domain of the Frizzleds, from where the signal diverges into one of the three pathways (Figure 3). It has been proposed that coupling of particular Wnt and Frizzled isoforms, as well as the presence of co-receptors, determine the activation of the specific Wnt pathway, where Dvl plays a crucial role as a molecular

switch with respect to the signal perceived (Kohn and Moon, 2005). Among the 19 Wnt proteins that have been identified in mammals, Wnt3a and Wnt5a are widely recognized as activators of the canonical and non-canonical pathways, respectively (Huang and Klein, 2004) (Jin, 2008). In addition, coupling of specific Wnt ligands with their receptors in disparate organisms and cell lines identified so far, as well as the outcome of such couplings can be found in Appendix Table 1.

In the inactive canonical pathway, the β-catenin destruction complex formed by AXIN, adenomatous polyposis coli (APC), and the serine threonine kinase glycogen synthase kinase 3beta (GSK3β), phosphorylates β-catenin on its N-terminal domain. Phosphorylated β-catenin is targeted for polyubiquitination and degradation by the proteasome. In the absence of β-catenin, Wnt target genes are repressed by the complex formed from the partnering of Groucho and lymphoid enhancer factor/T cell factor proteins (LEF/TCFs), which through binding Wnt response elements (WRE) blocks transcription (Gordon and Nusse, 2006). On the other hand, the canonical pathway is activated upon Wnt binding to Frizzled and its co-receptor low density lipoprotein related protein 5 or 6 (LRP5/6), which recruits Dvl. Dvl further interacts with the components of the β-catenin destruction complex, in which β-arrestins are proposed to facilitate this interaction through an unknown mechanism (Force et al., 2007). This interaction is stabilized through AXIN's binding to the cytosolic tail of LRP5/6, which is phosphorylated by GSK3β. When the β-catenin destruction complex is bound by Fzd-LRP5/6-Dvl components, β-catenin is stabilized in the cytoplasm and is subsequently translocated into the nucleus, where it displaces Groucho and partners with LEF/TCFs, activating the transcription of the Wnt target genes (Daniels and Weis, 2005). In addition,

secreted Frizzled related protein 1 (sFRP1) and Dickkopf (Dkk) family members have been identified as antagonists for the canonical pathway, where Dkk1 is thought to inhibit signaling through the canonical pathway by binding to the extracellular domain of LRP6 (Hermann et al., 2007) (Schinner et al., 2008) (Krupnik et al., 1999).

In the case of non-canonical signaling pathways composed of the PCP and the Wnt/Ca^{2+} signaling pathways, the studies mostly performed on *Drosophila* and *Xenopus* identified their involvement in tissue polarity, cell migration, and cytoskeleton rearrangements, where the role of these pathways in mammalian systems are not clear (Kikuchi and Yamamoto, 2008). However, extensive cross-talk between the Wnt pathways are thought to occur based on the fact that these pathways share components with signaling pathways mediated by classical 7 transmembrane receptors (7TMRs) involving the small guanosine 5'-triphosphate (GTP) binding proteins (G-proteins) Rac and Rho activating the c-Jun N-terminal kinase (JNK) and Rho-associated kinase (Rho-kinase) in the PCP pathway, respectively, as well as the coupling of G-proteins with Fzd in activating the Wnt/Ca^{2+} pathway (Dupre and Hebert, 2006) (Figure 3). One example of such cross-talk has been shown to occur through the secondary messenger Ca^{2+}, where $[Ca^{2+}]_i$ are shown to be increased through the activation of Wnt/Ca^{2+} pathway, which induces modifications of calcium-sensitive proteins calcium calmodulin-dependent protein kinase II (CamKII) and PKC (Kohn and Moon, 2005) (Figure3). In elevated calcium concentrations, CamKII binds and phosphorylates TAK1, which is a mitogen activated protein kinase (MAPK) kinase kinase (MAPKKK) that in turn activates NLK (a MAPK). Active NLK phosphorylates TCF, which inhibits the formation of β-catenin-LEF/TCFs complex, turning the Wnt target gene synthesis off (Kohn and Moon, 2005).

Therefore, some groups have categorized Fzds as atypical 7TMRs due to their coupling with G-proteins forming platforms for extensive cross-talk within the Wnt pathways, as well as between the Wnt and other signaling pathways mediated by classical 7TMRs (Force et al., 2007).

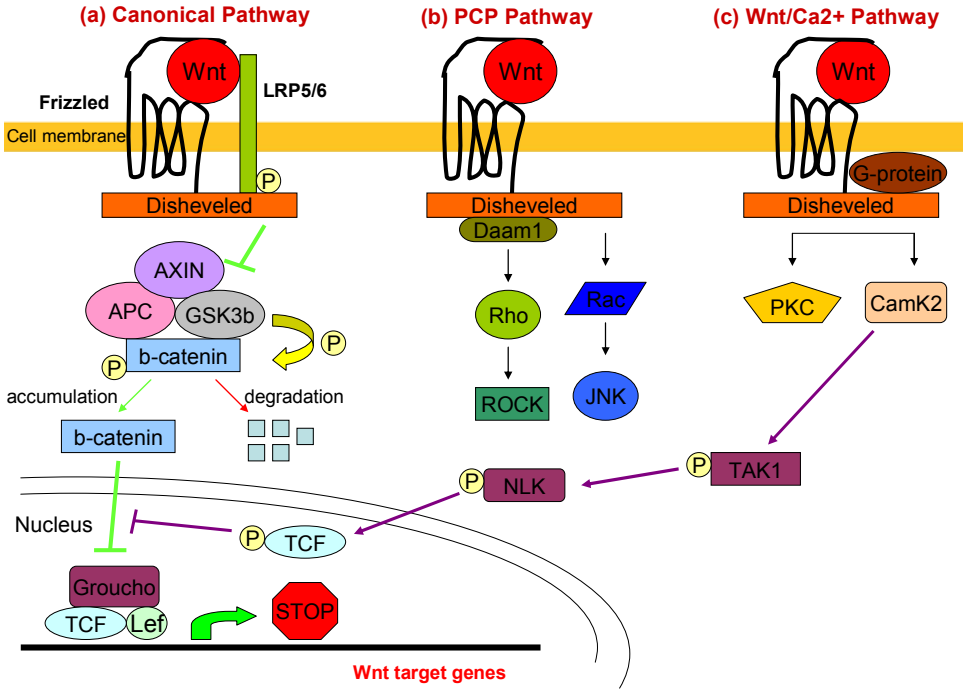

Figure 3. The Wnt signaling pathway. Three Wnt signaling pathways are depicted. Green arrows indicate the path when the canonical pathway is active, whereas red arrow points out proteosomal degradation of β-catenin when the pathway is inactive (a). Crosstalk between the pathways enabled through MAPK signaling is color coded in purple.

Recent functional and genomic studies have linked several components of the Wnt pathway to the development of T2DM, such that the *Wnt5b* gene was shown to be highly associated with this disorder in Japanese subjects (Kanazawa et al., 2004). However, the strongest genetic evidence comes from association studies performed on the gene *TCF7L2* that encodes for LEF/TCFs family member TCF-4 (Molenaar and Destree, 1999). The allelic variants within the *TCF7L2* were found to be consistently

associated with the development of T2DM through independent studies performed on major ethnic groups including Europeans, Japanese, Indians, Mexican Americans, West and North Africans (Cauchi et al., 2007), (Smith, 2007), (Hattersley, 2007), (Palmer et al., 2008). These studies have revealed consistent associations of the risk T allele in single nucleotide polymorphisms (SNPs) rs7903146 and rs12255372 with impaired insulin secretion (Lyssenko et al., 2007). In line with these findings, a recent report has revealed that depleting *TCF7L2* from isolated human and mouse pancreatic islets impaired GSIS, suggesting a link between the genetic evidence and the pancreatic beta-cell function with respect to the onset of T2DM (Shu et al., 2008). The importance of the co-receptor *LRP5* in beta-cell function has been implicated through functional studies, where *LRP5* deficient mouse islets have shown to give rise to impaired GSIS even in the presence of exogenous Wnt3a stimulation (Fujino et al., 2003). Additionally, the essential functioning of the Wnt signaling pathway in mouse pancreas was shown through the expressions of *Wnt2b, 5a, 5b, 7b, 11* and *Fzd2, 3, 4, 6, 8, 10* during embryonic developmental stages and after birth, where *Wnt1, 5a, 5b* and *Fzd 2, 3, 7* have determined to colocalize with insulin expressing cells (Heller et al., 2002). Similar findings were reported on the expressions of *Wnt2b, 3, 4, 5a, 7b, 10a, 14* and *Fzd 1-7* in isolated human islets, where all of the Fzd isoforms were found to colocalize with the islets of Langerhans (Heller et al., 2003).

The evidence of an active Wnt signaling pathway through the expression of several Wnt and Fzd isoforms in the endocrine mouse and human pancreas, as well as the few Wnt signaling pathway components with identified roles in glucose-stimulated secretion form the basis of our interest in this pathway. Therefore, the delineation of the

Wnt signaling pathway in relation to insulin secretion forms one of the aspects of my thesis project.

The Insulin Resistance Atherosclerosis Family Study (IRASFS):

The Insulin Resistance Atherosclerosis Family Study (IRASFS) is a biethnical epidemiological cohort study that aims to determine the underlying genetic components, as well as the environmental risk factors in the induction of insulin resistance (Henkin et al., 2003). In this respect, families of Hispanic descent from San Antonio, Texas, and San Luis Valley, Colorado, in addition to families of African American descent from Los Angeles, California, were recruited based on large family size, rather than the affection status of individuals from extreme phenotypes like diabetes (Palmer et al., 2006). Following recruitment, a clinical examination was performed, where the frequently sampled intravenous glucose tolerance test (FSIGT) was utilized to measure insulin sensitivity (S_I), acute insulin response (AIR), and disposition index (DI), which form the quantitative measures of glucose homeostasis (Palmer et al., 2006). In particular, S_I and AIR directly correlate to insulin resistance and beta-cell function, respectively, in intact organisms (Bergman et al., 2002), and thus form crucial components of the study design in the molecular genetic analysis, stated in Table 1.

Table 1. Properties of IRASFS subjects. Means ±standard deviation (median)

	African American	Hispanic
Pedigrees	42	86
Individuals	603	1261
Gender (% Female)	59.7	58.8
Age (years)	42.9 ± 14.0	42.7± 14.5 (41.2)
Diabetes (%)	12.3	12.7
BMI (kg/m^2)	30.0 ± 6.8 (29.0)	28.3 ± 5.8 (27.6)
AIR: Acute Insulin Response (pmol/l)	1003 ± 826 (769)	761 ± 650 (588)
S_I: Insulin Sensitivity ($x10^{-5}min^{-1}/pmol/l$)	1.63 ± 1.17 (1.41)	2.2 ± 1.9 (1.7)
DI: Disposition Index ($x10^{-5}min^{-1}$)	1423 ± 1269 (1150)	1320 ± 1238 (1008)
Fasting Glucose (mg/dL)	94.6 ± 9.7 (93.0)	93.4 ± 9.5 (92.0)

N. Palmer, personal communication.

Table 1. Properties of IRASFS subjects. The structure of the recruited families is depicted in the table. Since the recruitment of the individuals was based on a large family size, approximately 12% from each group were affected with diabetes. It is observed that African American subjects are more insulin resistant than Hispanic American subjects, however this resistance is compensated with increased insulin secretion in African Americans as depicted in AIR measurements.

Among the characteristics of glucose homeostasis measures, AIR measurement represents the acute phase of insulin secretion in response to elevated glucose concentrations, described under the pancreatic beta-cell function section. On the other hand, S_I measurements reflect beta-cell response to varying glucose concentrations, in which a decreased sensitivity points out to inhibited insulin action due to increased insulin resistance, leading to enhanced insulin secretion to maintain normal blood glucose levels forming the initial developmental states of T2DM, as mentioned earlier. DI is an accurate tool in assessing the correlation of insulin sensitivity to insulin secretion that yields a quantitative measure of the beta-cell's ability in compensating for insulin resistance (Bergman et al., 2002). This measurement is calculated by the multiplication of S_I and AIR measurements obtained from the subjects.

Linkage analysis of quantitative trait loci (QTL) for measures of glucose homeostasis followed by finemapping revealed DI and AIR loci, which mapped to chromosome 11q in the IRASFS African American families (Palmer N.D., 2006). Linkage was observed for DI on chromosome 11q at 80cM. This peak was flanked by a

bimodal AIR linkage peak encompassing a large genomic interval on chromosome 11q. Taken together, this suggests the involvement of multiple genes for linkage with the measures of glucose homeostasis (AIR and DI) in this genomic region (Palmer et al., 2006). As a follow-up of these linkage analyses, a dense SNP map was constructed and single SNP association to each quantitative phenotype were performed using two statistical genetic analysis methods: Sequential Oligogenic Linkage Analysis Routines (SOLAR) and Quantitative Pedigree Disequilibrium Test (QPDT). SOLAR is a computer software that has a variance component measured genotype approach that is used in SNP analysis (Almasy and Blangero, 1998). On the other hand, QPDT is used to detect linkage disequilibrium between a genetic marker and quantitative traits in general pedigree and is generally robust to potential population stratification (Dudbridge, 2003). In this respect, Table 2 summarizes the prioritization criteria for the genes within chromosome 11q that fall under AIR and DI linkage peaks.

Table 2. Prioritization scheme and number of loci based on detailed molecular genetic analysis of chromosome 11.

	Prioritization criteria						
Priority	Trait	Test	Location	P-Value for Association	# of Independent Loci	Cummulative Number of loci	Gene(s)
Genic loci							
1	AIR **and** DI	QPDT **and** SOLAR	Gene	<0.01	1	1	*GAB2*
2	AIR **and** DI	QPDT **and** SOLAR	Gene	<0.05	0	1	-
3	AIR **and/or** DI	QPDT **or/and** SOLAR	Gene	<0.001	1	2	*MRPL48*
4	AIR **and/or** DI	QPDT **or/and** SOLAR	Gene	<0.01	7	9	*see appendix 2*
5	AIR **and/or** DI	QPDT **or/and** SOLAR	Gene	<0.05	8	17	*see appendix 2*
6	AIR **or** DI	QPDT **or** SOLAR	Gene	<0.001	1	18	*see appendix 2*
7	AIR **or** DI	QPDT **or** SOLAR	Gene	<0.01	1	19	*see appendix 2*
8	AIR **or** DI	QPDT **or** SOLAR	Gene	<0.05	30	49	*see appendix 2*

Table 2. Prioritization scheme and number of loci based on detailed molecular genetic analysis of chromosome 11. Table of results used for the prioritization of the genes under chromosome 11q linkage peaks of DI and AIR are shown. These analyses were performed at Dr. Donald W. Bowden's laboratory, where genes associated with AIR and DI in both statistical analysis approaches of QPDT and SOLAR at a p-value of less than 0.01 were give the highest priority. As seen, *GAB2* is the only gene for such association. As the list extends, the criteria for association become less stringent. In line with this, the number of genes included in the association increases. The complete list of genes can be found in Appendix Table 2.

Using a prioritization scheme that maximized trait-trait and test-test overlap, genes within the linkage interval were prioritized based on statistical significance (Table 2). In this way, the prioritization of genes under the chromosome 11q linkage peaks revealed 24 candidate genes as contributors to the variation in glucose homeostasis measures and thus making them candidates directly involved through AIR or indirectly involved through DI in the beta-cell function. Therefore, as a part of my thesis, these genes have been screened via the cell-based surrogate assay, in an attempt to provide functional evidence for the association data obtained from Dr. Donald W. Bowden's laboratory. A complete list of these genes with their known functions can be found in Appendix Table 3.

METHODS

Cell culture:

INS1-E rat pancreatic beta-cells are maintained in Roswell Park Memorial Institute (RPMI) medium that is supplemented with 5% fetal bovine serum (FBS) and are split every 3-4 days. All cells are grown at 37^{o}C. 1-2-dimyristyloxypropyl-3-dimethyl-hydroxy ethyl ammonium bromide and cholesterol (DMRIE-C) is used as cationic lipid reagent to transfect INS1-E cells, as described in detail below. The average transfection efficiency determined from INS1-E cell transfections is approximately 28%.

The media used in cell culture including phosphate-buffered saline (PBS), OPTIMEM, RPMI and Dulbecco's Modified Eagle Medium (DMEM) are obtained from Wake Forest University's Cell Core Facility, whereas Krebs solution is made fresh containing 140mM NaCl, 3.6mM KCl, 0.5mM NaH_2PO_4, 0.5mM $MgSO_4$, 1.5mM $CaCl_2$, 2mM $NaHCO_3$, 10mM Hepes (pH 7.35) and 0.1%BSA.

siRNA:

The synthetic siRNAs used in our cell-based assays are designed by Dharmacon, which applies the following criteria to minimize the inadvertent gene modulations described under siRNA section (Echeverri et al., 2006):

1) Targeting siRNAs against all known splice variants of a given gene within the desired organism, where cross-checking with the SNPs database (dbSNP) is a requirement to ensure specificity in the intended gene knock-down by discarding SNP positions from the siRNA design.

2) The presence of palindromic sequences, high GC content, long chain of individual bases and "GTCCTTCAA" motif are avoided in the designs, due to their involvement in

internal secondary structure formation, prevention of duplex unwinding, decreased specificity in hybridization and in the induction of IFN response, respectively.

3) A threshold of two nucleotide mismatches between the siRNA and a non-target mRNA sequence is set to abolish off-targeted gene silencing.

Additionally, for siRNAs designed against the Wnt signaling components, the designed sequences are BLASTed against the rat genome in order to make sure that each siRNA targets the specific gene of interest and that each siRNA sequence contains at least three mismatches with the next similar gene it complements with.

Surrogate Assay for pancreatic beta-cell insulin secretion:

The surrogate assay is based on the strategy of robust estimation of insulin release using a secretory granule targeted alkaline phosphatase (SAP) vector as the marker for secretion. INS1-E rat pancreatic beta-cells that are transfected with the SAP vector secrete alkaline phosphatase along with insulin into the cells' media upon glucose stimulation, in which the activity of this enzyme can be measured using its colorimetric substrate 4-nitrophenyl phosphate, which will be referred to as SAP activity throughout the text. In line with this estimation of secretion approach, the pancreatic beta-cells are co-transfected with siRNAs and nuclear targeted red fluorescent protein (ntRFP) vector along with the SAP vector on a 96-well plate format, in which the ntRFP vector is used to determine the transfection efficiency. siRNAs and DNA vectors are delivered into the cells via a cationic-lipid mediated transport using DMRIE-C reagent from Invitrogen that is composed of the cationic lipid DMRIE and cholesterol, in equimolar amounts. In the transfection media, DMRIE-C readily forms complexes with the DNAs and siRNAs referred to as "lipoplexes", which are thought to be conveyed to the nucleus through the

cell's endocytotic machinery (Zuhorn et al., 2007). In our assays, the transfection mix per well is composed of 2.5μM siRNA (or no siRNA for control samples), 16ng of the ntRFP vector and 48ng of the SAP vector in 25μL of OPTIMEM, which are mixed with 0.375μL DMRIE-C reagent in 25μL of OPTIMEM. This mix is incubated at room temperature for 40 minutes. INS1-E rat pancreatic beta-cells are counted and added to each well to make 100 thousand cells in a total volume of 100μL of OPTIMEM that are subject to overnight incubation at 37^{o}C. Followed by this incubation, the cells are placed in the growth media (RPMI) for 3 days prior to glucose stimulated secretion. At the end of the third day, cells are first imaged to detect the transfection efficiency through ntRFP vector. After imaging, they are washed twice with Krebs solution supplemented with 2.5mM glucose and placed in this solution for a 40 minute pre-incubation (this pre-incubation step was not performed on the secretion assays for the screens of IRASFS genes and the wash step was performed with Krebs solution without glucose in these screens). Following pre-incubation, the cells are stimulated with Krebs solution in 16mM glucose concentration except for the negative controls that are stimulated with Krebs solution supplemented with 2.5mM glucose. The glucose stimulation in varying concentrations (2.5mM and 16mM glucose in Krebs solution) is performed over a three hour period at 37^{o}C. At the end of the third hour, 75μL of the Krebs media with varying glucose concentrations are taken out into a new 96-well microtiter plate, in which 75μL of p-nitrophenyl phosphate tablets from SIGMA dissolved in 2X glycine buffer is added in each well in order to measure the SAP activity, where one SIGMA tablet is reconstituted in 5mL of 2X glycine buffer. This activity is measured at an absorbance of 405nm every 10 minutes over a period of 2 hours. The rate of secretion for each well is

determined by subtracting the SAP activity value at the end of the 2nd hour's measurement from the SAP activity of the first measurement. The calculated rate of secretion is used in the data analysis as described below.

In each secretion experiment, the surrogate assay can accommodate the knock-down of 17 distinct genes through their specific siRNAs in 4 replicas and the effect of each silenced gene in beta-cell secretion can be assessed by comparing its SAP activity to that of 8 wells of negative controls (stimulated with low glucose concentration) and of 16 wells of positive controls (stimulated with high glucose concentration); each lacking siRNAs in their transfection components, with an addition of 2 wells of untransfected cells. Due to the fact that glucose concentrations less than 5mM are determined to be "unstimulatory" (Newgard and McGarry, 1995) and at 10mM glucose concentration, cells have been shown to perform their maximum insulin secretion (Antinozzi et al., 2002), 2.5mM and 16mM glucose concentrations are used to stimulate the negative and positive controls, respectively. On the other hand, the knocked-down components, as well as the untransfected cells are stimulated with high glucose concentration to create a platform of comparison on insulin release at the maximal secretion capacity of the beta-cells. In this respect, the untransfected cells reflect the background noise of the assay due to the fact that there should be no SAP activity measured in the media of these cells. Therefore, the surrogate assay for beta-cell secretion forms a novel high-throughput screening strategy that estimates secretion specifically from the transfected cells, which enhances the power to assign individual genes a pertinent role in secretion.

Cell imaging:

BD pathway 855 is used in imaging cells. The cells in surrogate assays are imaged three days post-transfection to determine the transfection efficiency prior to the initiation of secretion experiments. In this respect, Alexa 594 channel is used to detect the intensity of the ntRFP vector, which resides in the nuclei of the transfected cells. Following secretion assays, cells in the 96-well plates are washed once with 1X PBS and are placed in 1:4000 diluted Hoechst dye (Molecular Probes 33342) in 1X PBS for at least 20 minutes. Hoechst is a nuclear stain whose intensity is measured by the Hoechst channel in the imaging system to determine the cell number in each well. In addition, transmitted images of 96-well plates are taken to visualize any potential problems in each well. For each experiment, there is at least one image for Hoechst or Alexa 594 channels that were captured in a montage (4x4, 2x2 or 3x3), enlarging one spot on the well, or a specific spot within the same well was captured with an offset value of 250. However, for some experiments, more than one image was available per well for either channel using one of these features of capturing.

Data analysis:

a. Image analysis:

Image analysis is composed of two steps: thresholding and image quantification.

In the first step, appropriate threshold values for the intensities of Hoechst stained images and for the ntRFP vector are determined using Image J program. In this respect, thresholds are determined from the untransfected cells. In the case of Hoechst staining, the minimum threshold value that distinguishes the cells' nuclei from the background is recorded from the images detected by Hoechst channel. In contrast, maximum threshold

value is recorded from Alexa 594 channel measurements of the untransfected cells, since these cells do not contain ntRFP vector and thus the intensity detected in this channel would represent the background noise of the assay. The recorded threshold values are multiplied by 1.2 to ensure the elimination of any well to well imaging variability by 20% so that the threshold values are set above the background. Figure 4 depicts cell images along with examples of thresholding.

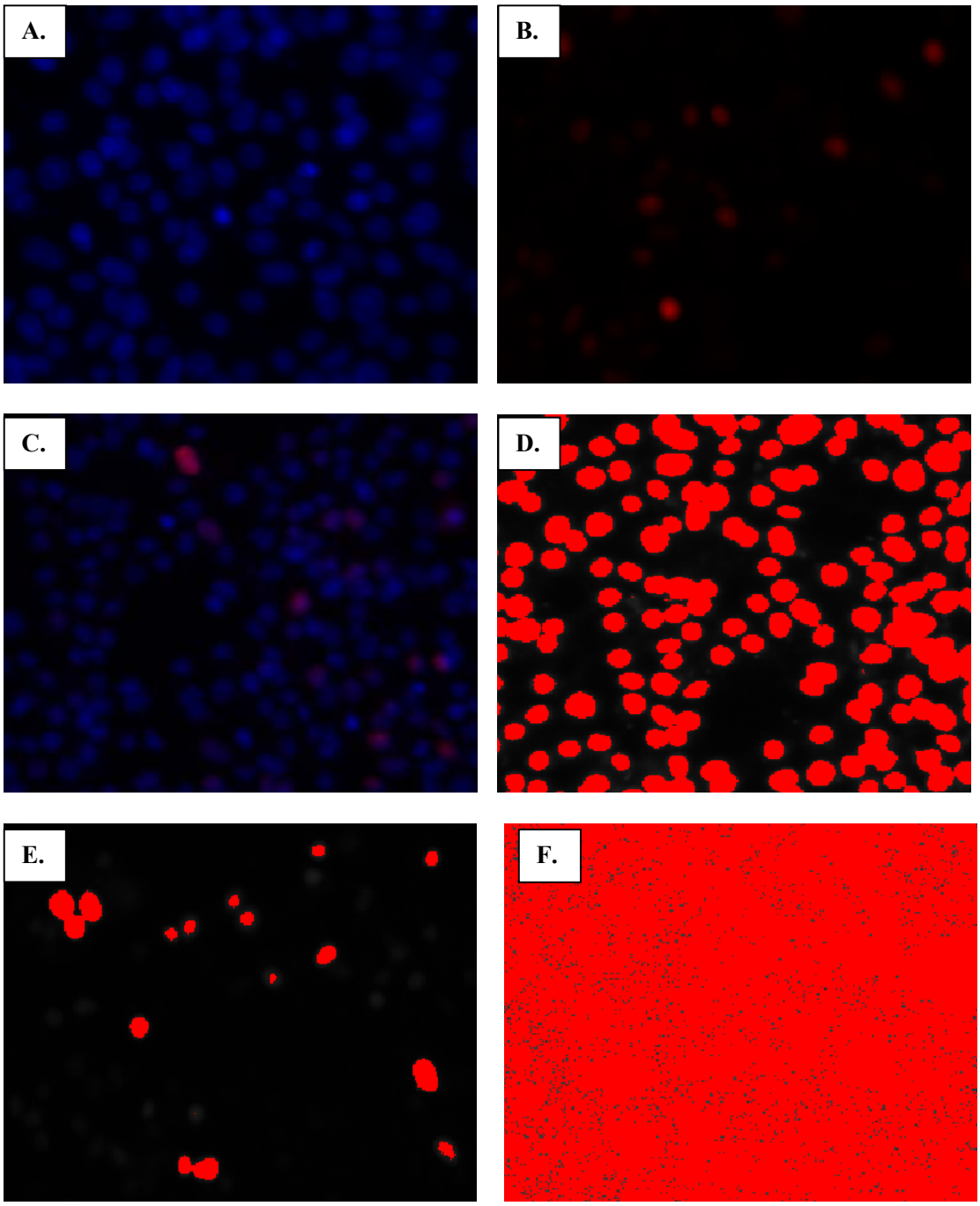

Figure 4. Cell imaging. A. The visualization of Hoechst stained cells. The cells are represented by blue color. **B.** ntRFP transfected cells are determined by Alexa 594 channel and are depicted in red color. **C.** Merged images of Hoechst (A) and Alexa 594 (B) channels, showing the transfected cells in magenta color. **D.** An example of thresholding for Hoechst stained cells. The red dots represent the cells that are distinct from the background. The minimum threshold value for this image is determined to be 559 by Image J program. On the other hand, thresholding for Alexa 594 channel for transfected (**E**) and untransfected (**F**) cells are depicted. For image quantification, the maximum threshold value of the untransfected cells are used, which in panel **E** is determined to be 257 by Image J program.

In the second step of analysis, the multiplied threshold values are placed into an automated image analysis script established by Dr. Peter A. Antinozzi, which calculates the area in pixels of the measured intensities from Hoechst and Alexa 594 channels. These areas from Hoechst and Alexa 594 channel measurements are used to normalize secretion data to cell number and to provide secretion data as a true reflection of the transfected cells referred to as transfection efficiency, respectively. In line with this approach of data analysis, each well is compared across its data points obtained from the calculated areas from Hoechst and Alexa 594 channels and the secretion rate acquired by the slope of the measured SAP activity. From these comparisons, the outlier data points within the image analysis are determined on a well-well basis. The wells having areas of zero pixels from either of the channels in focus are eliminated –except for Alexa 594 channel in untransfected cells-, since this value indicates absence of cells and inadequate transfection efficiency for Hoechst and Alexa 594 channels' measurements, respectively. Additionally, aberrantly high or low values of calculated areas are checked with their corresponding images prior to exclusion from the data analysis. For experiments where only a single image from either channel is available, the outliers determined this way lead to the exclusion of the secretion rate along with the image analysis pertinent to the specific well with aberrant values of calculated areas. However, assays having multiple images per well provided an option of comparison among these images in order to come to a conclusion in the outlier determination. In such a case, factors like imaging errors due to a bright spot on the well or loss of cells due to handling during secretion assays helped us deduce whether to exclude the whole well from the analysis or just to eliminate specific image data and retain the secretion rate for the analysis.

b. Pooling independent assays:

Following the elimination of outliers, the quantified images and the data obtained from secretion assays are incorporated to pool independent experiments. Within each experiment, the rate of secretion per well is divided by the Hoechst area calculated for that well in order to normalize SAP activity to cell number. Each well belonging to the same sample is then averaged to represent its estimated insulin release, i.e. the SAP activity for that sample. Independent experiments are pooled by normalizing each assay to its high glucose control by taking the difference between the normalized SAP activity of each sample and the SAP activity of untransfected cells, and dividing it by the difference between the SAP activities of high glucose control and untransfected cells. On the other hand, the calculated areas from Hoechst and Alexa 594 channels are averaged for each sample within individual assays. These averaged values from independent assays are pooled together by dividing each sample's area by the area obtained from high glucose control. This way, the cell number and transfection efficiency is set to 100% in high glucose controls providing a platform for pooling the imaging data.

A final step of data elimination took place by determining outliers within the pool of SAP activity normalized to cell number from independent assays. In this respect, z-score is calculated for each sample that has high standard deviations from the mean of pooled results. Additionally, probability of a defect in the individual data points depending on the calculated z-score was determined using the "=normsdist(z-score)" formula in excel, which determines the percent probability of encountering a defect in the specific data point. In this respect, 0.9 and 82% were set as threshold values for z-score and probability

of a defect, respectively. Hence the samples having z-scores and probability of a defect exceeding the threshold values are discarded from the final analysis.

On the other hand, since there is no imaging data available for the initial secretion assays performed on IRASFS genes, independent experiments are pooled by normalizing the SAP activity to high glucose control only within each assay. This is accomplished by subtracting the SAP activity for each sample from the SAP activity of the low glucose control that is divided by the difference between the SAP activities of high and low glucose controls. In this way, secretion is set to 100% and 0% for high glucose and low glucose controls, respectively, enabling a normalization measure to pool independent assays together.

c. Statistical analysis:

In the final step of data analysis, analysis of variance (ANOVA) is used as our statistical approach on the pooled data. ANOVA enables the simultaneous analysis of differences between two or more sample means and yields a comparison matrix based on F-statistics. From this matrix, F ratios of samples to each other can be obtained. The F ratios for each sample to the high glucose control are acquired from this matrix in order to determine the samples that significantly deviate from the control. Additionally, the standard look-up ANOVA tables are used to calculate F critical values by setting a limit on the p-value for significance. Depending on the p-values of choice, the number of comparisons and total data points, F critical values vary, setting the threshold for significance. In this respect, the F critical values are determined for each experiment at a p-value of 0.05 and denoted in the respective figure. Significance is assumed in samples with F ratios that exceed the calculated F critical values.

Quantitative real time-polymerase chain reaction (qRT-PCR):

qRT-PCR is used to corroborate the findings of the secretion assays, where the content of gene knock-down is quantified. In this respect, total RNA is isolated using Qiagen RNeasy Mini Kit at the end of the secretion assays by pooling 4-6 wells belonging to the same sample and is used in the synthesis of complementary DNA (cDNA). To detect gene expression, approximately a 200bp region of the gene of interest is amplified via the primers that are designed to span exon-intron boundaries. The rationale behind this design is to eliminate any genomic DNA contamination. The RT-PCR reactions are performed in ABI 7500 Real Time PCR System, where the detection of the amplified sequence during RT-PCR is established through SYBR Green I, which is a fluorescent dye. This dye intercalates into double stranded DNA (dsDNA), leading to an increase in its fluorescent emission compared to its unbound state. Therefore, during the elongation step of each cycle, the fluorescent measurements are recorded, yielding the increase in the fluorescence in parallel to the accumulated PCR amplicons.

The cDNA synthesis from the RNA isolates is accomplished through Clontech's ready dT-oligo mixes, comprised of primers, reverse transcriptase, and deoxyribonucleotide triphosphates (dNTPs), lyophilized in an $MgCl_2$ containing reaction buffer. The RNA isolates are diluted to reach a concentration of 0.025μg/μl, where 20μl of this dilution is added to the ready mixes prior to incubation at 42^{o}C for 90 minutes. Heating the samples at 70^{o}C for 10 minutes terminates the reaction, forming the cDNA. A 1:20 dilution of the cDNA is then used in the RT-PCR reaction along with the designed primers and SYBR Green I. Following RT-PCR, a dissociation curve analysis is performed, where the temperature is increased gradually starting from 60^{o}C up to 95^{o}C. Since SYBR Green

binds to dsDNA, the temperature that denatures DNA (melting temperature (T_m)), yields a loss of fluorescence; hence by plotting fluorescence against temperature, curves are obtained with peaks at their T_ms. A single peak would represent a reaction that is free of primer dimers and other non-specific products. Similarly, the sizes of the PCR amplicons are predicted on an agarose gel to ensure reaction specificity for each primer pair that is designed. In addition, each assay contains a negative control (-RT reaction) within the tested samples, where the RNA isolate is not reverse-transcribed into cDNA enhancing the power in detecting genomic DNA contamination.

In order to quantify gene expression in the samples, comparative C_t method ($\Delta\Delta C_t$) is applied to the data obtained from RT-PCR, where C_t stands for threshold cycle on a sigmoidal-shaped amplification plot of fluorescence versus the number of cycles. The amplification plot consists of background noise called the baseline, occurring in early cycles, and a threshold that is set above this noise. It is the intersection of this threshold to the amplification plot that determines the C_t value for each sample. These values are then used as comparison tools among the genes of interest and their controls lacking siRNAs, which are normalized to an endogenous housekeeping gene being the invariant control, i.e. having a constant C_t value regardless of the sample. The calculation is outlined as: $\Delta\Delta C_t = [(\Delta C_{t\ sample}) - (\Delta C_{t\ reference})$; where $\Delta C_{t\ sample}$ stands for C_t value of any sample normalized to the housekeeping gene and $\Delta C_{t\ reference}$ represents the C_t value of the control sample normalized to the housekeeping gene. A fold difference in expression can be acquired from $2^{\Delta\Delta Ct}$ formula.

qRT-PCR primers:

The following primers are designed using the web-based Clocs Oligo Designer program to amplify the specific gene indicated:

AXIN gene: *5'-GTGGATGGAATCCCCCCATACAGG-3'* and *5'-GCTGGACAGCCTCTAGACGGTG-3'* as forward and reverse oligos, respectively, span a 160bp region of the gene. T_m for both of the oligos is 60^oC.

β–catenin gene: The forward oligo *5'-GGAGTTGGACATGGCCATGGAGC-3'* and the reverse oligo 5'-*GCCCTTGCCACTCAGGGAAGG-3'*span a 126bp region of the gene with a T_m of 60^oC for both oligos.

GSK3β gene: *5'-GAACCGAGAGCTCCAGATCATGAG-3'* and *5'-CATAGATCACAGGGAGTGTCTGCTTGG-3'* are used as forward and reverse primers having T_ms of 59^oC and 61^oC, respectively. This primer pair amplifies a region of 190bp in the gene.

RESULTS

In order to fulfill the main objective of finding genes pertinent to pancreatic beta-cell secretory function, a high-throughput genetic screening strategy has been developed, as previously described in detail. This screening approach forms the basis of our study, since it is a robust way of detecting genes having significant impact on beta-cell secretory function, referred to as "hits". These hits guide us in narrowing down to a specific path in follow-up studies. Therefore, our initial experiment had the goal of demonstrating our method of estimation of insulin release as an accurate reflection on beta-cell secretion.

In line with this goal, a secretion assay was performed on INS1-E rat pancreatic beta-cells, co-transfected with the SAP and ntRFP vectors. The assay was carried out as described in the methods section with an additional component to the 3 hour period of cell stimulation, 50nM PMA. Since PMA has a potentiation effect in insulin secretion, it has been used with high (16mM) glucose control in order to provide a positive control to the experiment. In addition, untransfected cells are used to reflect the background noise of the assay, which were stimulated with 16mM glucose concentration (Figure 5).

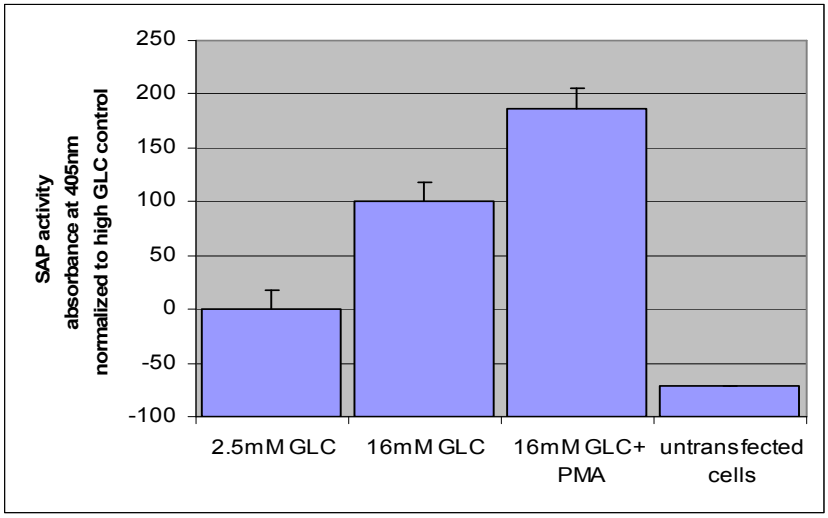

Figure 5. Glucose-stimulated SAP secretion parallels insulin release. Averaged SAP activity measurements for samples in 5 wells of low glucose, 6 wells of high glucose and 6 wells of high glucose and 50nM PMA are depicted. Additionally, SAP activity from one well of untransfected cells was determined. As shown, there is an approximate 2-fold SAP release caused by PMA

The results reflect estimated insulin secretion from each sample stimulated with low (2.5mM) glucose, high (16mM) glucose, high glucose with 50nM PMA and untransfected cells as SAP activities measured at an absorbance of 405nm. As observed, SAP secretion from each sample is glucose-stimulated and potentiated by PMA that leads to approximately 2-fold SAP release compared to high glucose stimulation alone. The fact that no SAP activity was detected from the media of untransfected cells indicates that the surrogate secretion assay specifically estimates insulin release from the cells that are transfected with the SAP vector.

Therefore, this assay is used in the screens of IRASFS genes and the Wnt signaling pathway components in order to identify genes involved in beta-cell secretory function. Our experimental approach involves large scale genetic screens using the secretion assay in order to determine hits, which helped us focus on particular IRASFS genes or a specific part of the Wnt signaling pathway for the follow-up analyses.

A. The Insulin Resistance Atherosclerosis Family Study (IRASFS) Genes:

Secretion assays were performed on the 24 IRASFS positional candidate genes, as previously described. The aim of the screens was to provide a functional validation to the genetic data, as well as to prioritize genes in terms of their impact on beta-cell secretion. Figure 6 depicts the results from 11 independent secretion assays performed on INS1-E cells, where each of the 24 genes was knocked-down using specific siRNAs and the results were pooled by normalizing the SAP activity to high glucose control as detailed under the methods section.

A.

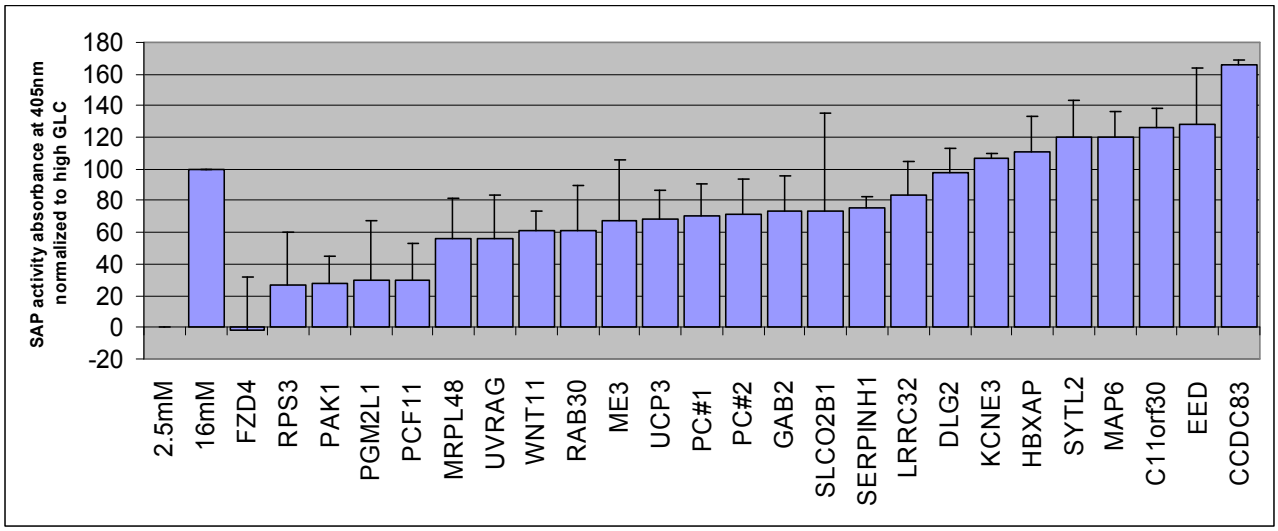

B.

$F_{critical}(0.05) = 1.56$			
Sample	**F ratio**	**Sample**	**F ratio**
*FZD4	55.5	*ME3	3.9
*PCF11	35.6	*PC#1	3.3
*RPS3	19.7	*PC#2	3.1
*PAK1	19.4	*SYTL2	3.0
*PGM2L1	18.3	*EED	2.9
*CCDC83	16	*MAP6	2.6
*MRPL48	11.8	*C11orf30	2.5
*UVRAG	11.6	*SERPINH1	2.3
*UCP3	6.1	Genes with F ratios below the critical value	
*WNT11	5.5	LRRC32	1.0
*RAB30	5.5	HBXAP	0.8
*SLCO2B1	5.0	KCNE3	0.2
*GAB2	4.3	DLG2	0.03

Figure 6. The screen on IRASFS genes. A. The graph depicts the SAP activity of the siRNA knocked-down IRASFS genes indicated on the x-axis along with the low (2.5mM) and high (16mM) glucose controls. The y-axis shows the percentage of secretion by the measured SAP activities at an absorbance of 405nm that are normalized to high glucose control, so that secretion in this control group is set to 100%. PC#1 and PC#2 represent two distinct siRNAs targeting the same gene (PC) for silencing. As seen, both siRNAs had similar effects on secretion. **B.** F ratios obtained from the comparison matrix following statistical analysis, ANOVA, is shown for each sample as their ratios to high glucose control. The F critical value is calculated to be 1.56 at a p-value of 0.05. * indicates samples that exceed the F critical value and are significantly different than high glucose control.

Figure 6A shows the effect of each silenced gene on beta-cell secretion as SAP activity measurements normalized to high glucose control, whereas in Figure 6B, the F ratio of each sample to high glucose control is calculated in addition to the F critical

value of 1.56 determined at a p-value of 0.05. The F ratio for any sample that exceeds the critical value is considered statistically different than the high glucose control, indicating a significant impact on glucose-stimulated secretion. Among these genes, knocking-down *FZD4* has the highest deviation from the control sample (Figure 6B), paralleling the profound inhibition in secretion (Figure 6A). Therefore, we have focused on the validation of this effect through follow-up studies, where image analysis has been used as our guide.

As a follow-up of our hit from the large scale screen of IRASFS genes, a secondary screen on *FZD4* was performed on INS1-E cells via the same siRNA that was used to knock it down in the initial screen of the IRASFS genes. Since our initial screen of IRASFS genes lacked image data, the follow-up screen was accompanied by imaging as an additional level of control, where the SAP activity obtained from the knock-down of *FZD4* was normalized to high glucose control and cell number. Figure 7 depicts these SAP activity results along with the imaging data that reveal cell number and transfection efficiency for each sample.

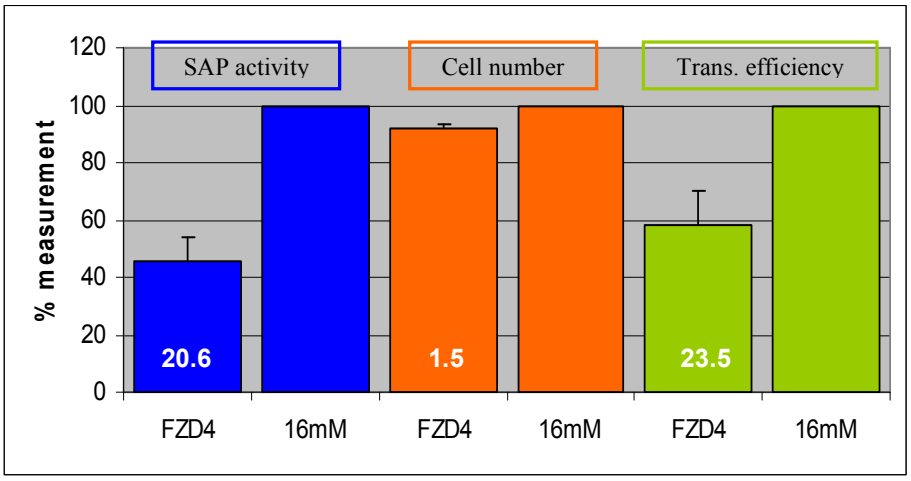

Figure 7. Follow-up analysis on *FZD4*. Depicted is the SAP activity measurement at an absorbance of 405nm, in addition to cell number and transfection efficiency as percent measurements in blue, orange and green bars, respectively. The results are pooled from 3-4 independent assays and normalized to high glucose control sample. The SAP activity measurements pooled from *FZD4* knocked-down and high glucose samples were normalized for cell number in their pertinent wells (blue). On the x-axis stands the knocked-down sample and high glucose control for each analysis depicted as *FZD4* and 16mM, respectively. F ratios of each sample to the high glucose (16mM) controls in their pertinent analyses are depicted as white numbers within the bars. The F critical values at a p-value of 0.05 are determined to be 2.5, 2.8 and 2.3 for secretion (blue bars), cell number (orange bars) and transfection efficiency (green bars) results, respectively.

A graph of multiple analyses is depicted in Figure 7, comprised of measured SAP activity, cell number and transfection efficiency represented by blue, orange and green bars, respectively. Each analysis on the knocked-down gene is illustrated with their corresponding high glucose control that they are normalized, in order to show percent measurement on the y-axis. The abbreviations of *FZD4* and 16mM on the x-axis of the graph stand for the knock-down and high glucose control samples, respectively, (Figure 7), in which the F critical values are distinct in agreement with the context of each independent analysis. The secretion data was normalized to high glucose control and cell number, in which the F ratio of the knocked-down *FZD4* sample to the high glucose control indicates that the inhibition in secretion is significant (Figure 7, blue bars). When the cell number is considered, an even distribution of cells was achieved among the

FZD4 knocked-down sample and the high glucose control (Figure 7, orange bars). In contrast, a significant reduction in the transfection efficiency was detected in the knocked-down sample, since the F ratio for this sample was found to highly exceed the F critical value of 2.3 determined for the transfection efficiency analysis. (Figure 7, green bars). Therefore, an accurate conclusion cannot be drawn about *FZD4*'s role in beta-cell function with this follow-up screen since the reduced SAP activity might be a result of low transfection efficiency.

In order to determine the role of *FZD4* gene in secretion, a new siRNA against this gene was designed to be utilized in the secretion assays. Image analysis was also performed in this follow-up analysis to validate the secretion results. In this respect, it is expected that transfection efficiency would not deviate significantly from that of high glucose control in order to verify the effect observed in secretion data. Figure 8 illustrates the secretion data normalized to high glucose control and cell number, as well as image analysis results from 3-4 independent assays, where *FZD4* silenced samples are compared to their corresponding high glucose controls.

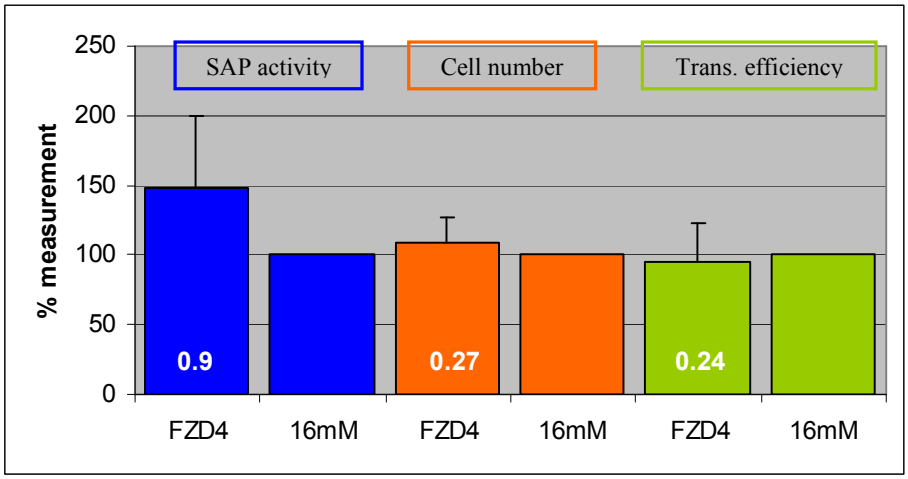

Figure 8. The follow-up of *FZD4* gene with an additional siRNA. Shown is the SAP activity measurement at an absorbance of 405nm, cell number and transfection efficiency as percent measurements in blue, orange and green bars, respectively. All results are normalized to high glucose controls as explained in the methods. Additionally, the SAP activity results were normalized for cell number (blue bars). The x-axis shows the knocked-down sample and high glucose control as *FZD4* and 16mM, respectively, for each analysis. F ratios calculated for FZD4 are indicated in white numbers within the bars. The F critical value is determined to be 1.7 at 0.05 p-value for all analyses.

As the results in Figure 8 suggest that the *FZD4* knock-down sample did not have a significant impact on secretion, since the F ratio calculated (0.9) does not exceed the determined F critical value (1.7) (blue bars). This result is further supported by the calculated cell number and transfection efficiency of the *FZD4* silenced cells that do not vary significantly from that of their high glucose controls (Figure 8, orange and green bars). Since the image data suggests no variation in cell number and transfection efficiency across the samples, it can be deduced that the knock-down of *FZD4* with the additional siRNA does not have an impact on glucose-stimulated secretion. Overall, due to the contradictory results observed so far, in order to draw a conclusion from the screens, further follow-up analysis confirming the gene knock-down should be included in the future studies.

B. The Wnt signaling pathway:

Despite the evidence supporting the involvement of the Wnt signaling pathway components *TCF7L2* and *LRP5* in the onset of T2DM, the role of the remainder of the Wnt signaling pathway components that facilitate signal transduction in pancreatic beta-cell function have not been identified. Therefore, our overall goal includes completing the picture of the Wnt signaling pathway with respect to their roles in insulin secretion.

In line with this goal, our approach contains an initial screen on the Wnt signaling pathway components, from which the hits obtained can be followed-up in order to unravel a general conclusion on the path to insulin secretion. In this respect, the components *GSK3β, β-catenin, AXIN, AXIN2, sFRP1, LRP5, LRP6, Wnt3a, Wnt10b* and *Dkk3* were knocked-down in INS1-E cells via their specific siRNAs and were subject to secretion assays, where secretion from each sample was reflected as SAP activity measurements. Figure 9 depicts the pooled results from 3-4 independent secretion assays, where the SAP activity was normalized to high glucose control and cell number. Additionally, imaging data from these assays have been provided in this figure, as a tool to increase confidence in secretion results.

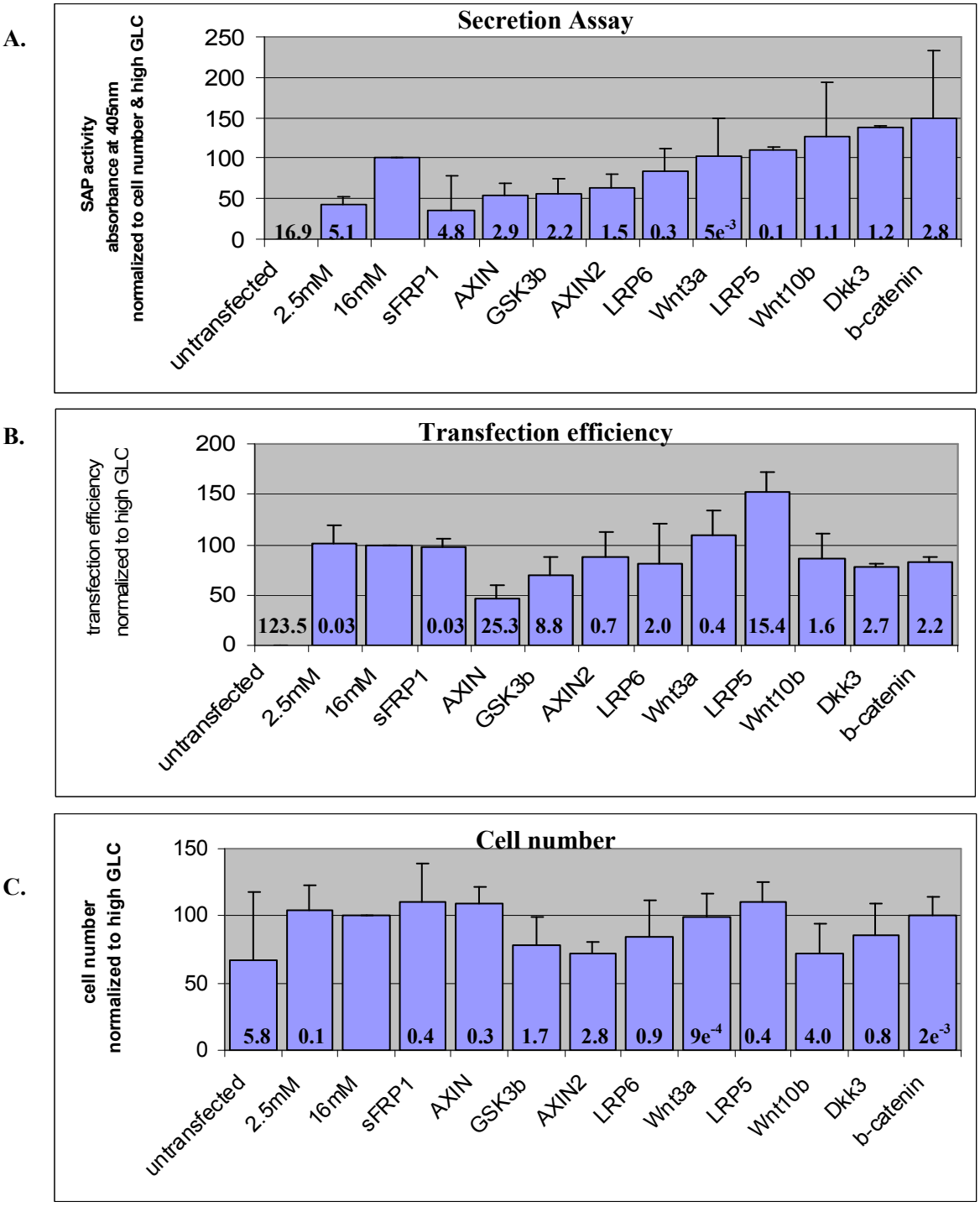

Figure 9. Initial screen on the Wnt signaling components. Figure depicts **A.** the secretion assay results normalized to cell number and high glucose control, where high glucose was set to 100% and untransfected was set to 0% **B.** and **C.** transfection efficiency and cell number, respectively, in which high glucose was set to 100% to enable a comparative platform across the samples. These results represent 3-4 independent assays. The F critical value is determined to be 1.7 at a p-value of 0.05 for each analysis illustrated in A, B and C. F ratios determined by the ratio of each sample to the high glucose control are presented within corresponding bars.

The secretion assay results suggest that the knock-down of Wnt components *sFRP1, AXIN* and *GSK3β* having F ratios of 4.8, 2.9 and 2.2, respectively, significantly inhibit glucose-stimulated secretion, since their F ratios highly exceed the calculated F critical value of 1.7 (Figure 9A). When the transfection efficiency on the samples is taken into account, the determined F-ratios in this analysis suggest significantly low transfection efficiency for *AXIN* and *GSK3β* knocked-down samples, whereas the *sFRP1* knocked-down sample shows a similar efficiency to high glucose control (Figure 9B). On the other hand, the secretion data reveals another hit in terms of increased glucose-stimulated secretion in the *β-catenin* silenced sample that has an F-ratio of 2.8 that exceeds the F critical value (Figure 9A). However, just like *AXIN* and *GSK3β* silenced samples, this hit also exhibits a significantly low transfection efficiency as supported with an F ratio of 2.2 (Figure 9B). In addition, the cell number for each well is depicted in Figure 9C, where all the hits mentioned, *sFRP1, AXIN, GSK3β* and *β-catenin*, show nearly constant distribution of cells across their corresponding wells, indicating that the low transfection efficiency in *AXIN, GSK3β* and *β-catenin* knocked-down samples is not due to low cell number. Depending on the imaging data, it can be implied that inhibited SAP activity observed in the *AXIN* and *GSK3β* silenced samples might be due to low transfection efficiency. However, this does not apply to the case of the *β-catenin* knock-down sample, where an enhanced secretion corresponds to low transfection efficiency. Therefore, in order to draw a conclusion, supporting evidence for the observed results should be provided.

In this respect, the knock-down of the genes *AXIN, GSK3β,* and *β-catenin* were quantified through qRT-PCR analysis. Since these genes are the main determinants for

the fate of Wnt target gene synthesis (Figure 3) and that the knock-down of *AXIN* and *GSK3β* significantly inhibited glucose-stimulated secretion as opposed to the effect observed by *β-catenin* knock-down, confirmation of the knock-down of these genes is essential in predicting their roles in beta-cell secretory function. Thus, qRT-PCR was performed on the total RNA isolates from the siRNA silenced and high glucose control INS1-E samples, where 6 wells per sample were pooled following one secretion assay. Figure 10 shows the result from the mRNA expressions quantified for the genes *AXIN, GSK3β, β-catenin, Cyclophilin A (CYCA)* and *Insulin*, which are normalized to the invariant control *CYCA* and to the high glucose control.

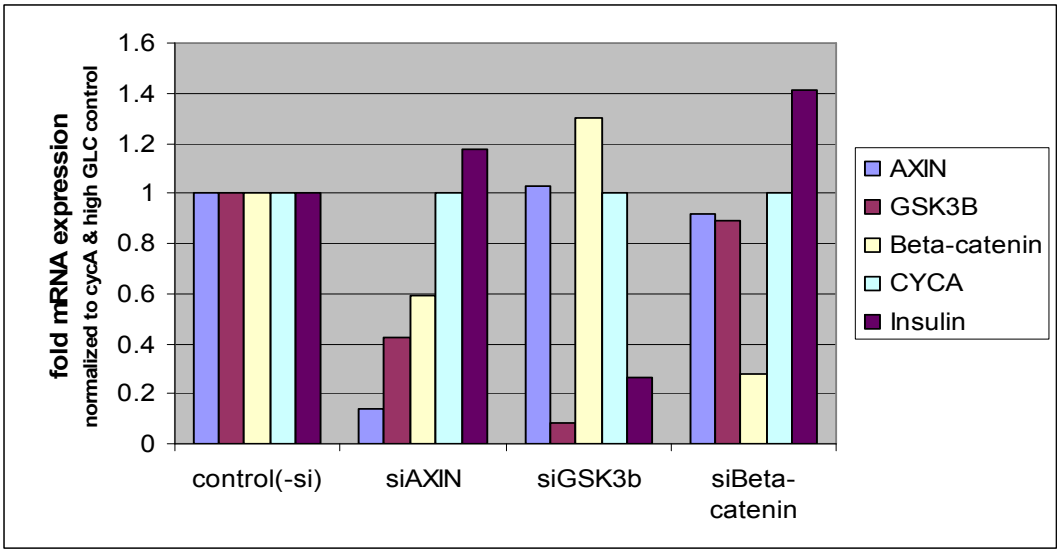

Figure 10. mRNA quantification on *AXIN, GSK3β* and *β-catenin* knock-down samples. Depicted in the diagram, fold mRNA expression levels normalized to the invariant housekeeping gene *CYCA* and the high glucose control are plotted against the samples transfected with siRNAs against the genes *AXIN*, *GSK3β* and *β-catenin* along with high glucose control (16mM) lacking siRNA presented on the x-axis. For each sample, the expression levels of the genes *AXIN, GSK3β, β-catenin, CYC A* and *Insulin* are quantified, shown in color coded bars.

The gene expression levels presented in Figure 10 are quantified as detailed in the methods section. The siRNAs against the genes *AXIN, GSK3β* and *β-catenin* were

calculated to inhibit the corresponding genes up to 86%, 92% and 72%, respectively, reflecting a successful knock-down of each gene.

Given that the *AXIN* gene was successfully knocked-down by its specific siRNA that was used in our initial screen, the next follow-up analysis involved knocking-down this gene with two additional siRNAs. These siRNAs were designed to target two different sequences on *AXIN* gene. The aim of this follow-up analysis is to confirm *AXIN*'s role in beta-cell secretion. In this respect, Figure 11 shows the results from 3-4 independent secretion assays normalized to cell number and high glucose control, in addition to image analysis determining transfection efficiency and cell number from these screens.

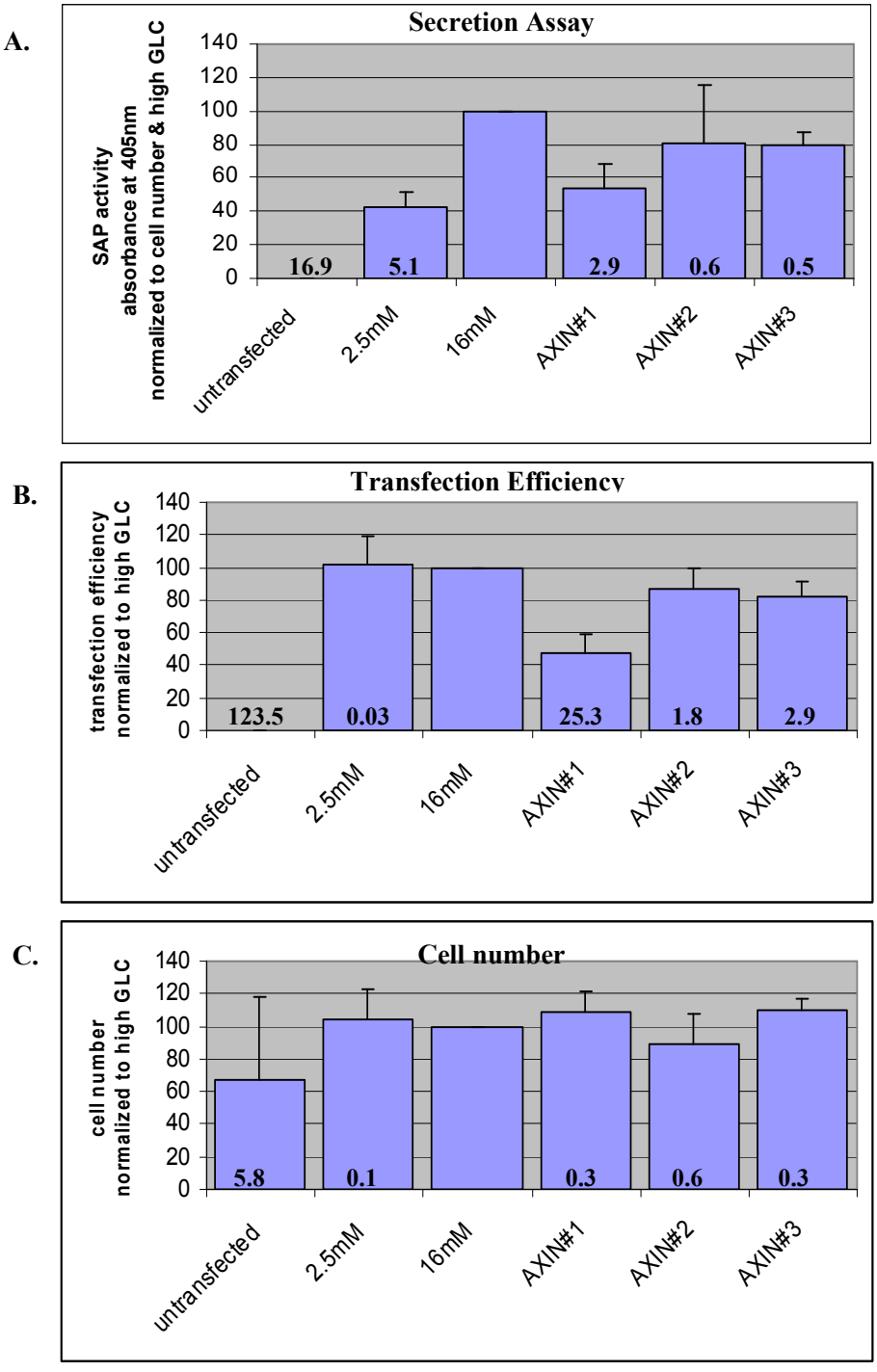

Figure 11. Follow-up on *AXIN* gene. The F critical value calculated for each assay is 1.7 at a p-value of 0.05. F ratios are stated in each analysis. F ratios that exceed the F critical value are considered to be significantly different than high glucose controls.
A. Secretion assay with components of untransfected cells, low glucose (2.5mM) and high glucose (16mM) controls, along with *AXIN* knock-down samples with three distinct siRNAs, are depicted as SAP activity normalized to cell number and high glucose control. AXIN#1 represents the siRNA used in the initial screen of Wnt components, where AXIN#2 and AXIN#3 are the newly designed siRNAs. The F ratios for each sample to high glucose control are stated within the bars.
B. Transfection efficiency for each sample is determined as detailed in the methods section. As seen, F ratios for each knock-down sample –except for low (2.5mM) glucose control- exceed the F critical value determined.
C. Cell number from each sample is represented. As the F ratios indicate, all samples, except for untransfected cells, have equal distribution of cells across disparate samples.

Figure 11 depicts the follow-up analysis on *AXIN* gene in secretion assay, transfection efficiency and cell number, where AXIN#1 represents the *AXIN* knock-down

sample with the siRNA used in the initial screen of the Wnt signaling components, and AXIN#2 and AXIN#3 stand for the additional siRNAs targeting this gene. As observed, only AXIN#1 sample significantly inhibits glucose-stimulated secretion, whereas the same effect was not detected in AXIN#2 and AXIN#3 samples (Figure 11A). On the other hand, the transfection efficiencies for all *AXIN* knocked-down samples are significantly lower than the high glucose control (Figure 11B) and that this effect was not due to low cell number in these samples (Figure 11C).

The fact that the screens performed with three different siRNAs against *AXIN* gene did not exhibit the same effect in SAP activity measurements lead us to investigate further the extent of gene knock-down by each of these siRNAs. In this perspective, qRT-PCR analysis was performed on *AXIN* knock-down samples and the results are shown in Figure 12.

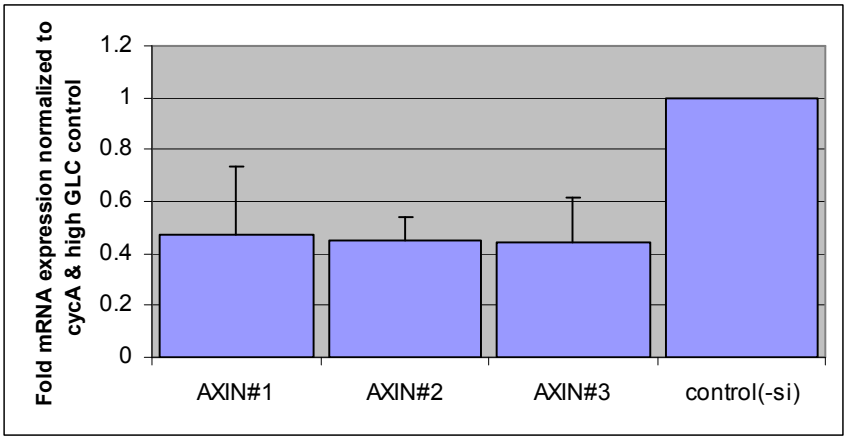

Figure 12. qRT-PCR analysis on *AXIN* knock-down samples. Depicted are the extent of *AXIN* knock-down by the three different siRNAs against it, normalized to the housekeeping gene *CYCA* and the high glucose (16mM) control. The results are pooled from 3-4 independent qRT-PCR analyses.
x-axis depicts 3 different siRNAs used in the follow-up of *AXIN* and the high glucose control that lacks siRNAs. The knock-down of each sample is nearly the same with an approximate inhibition of 45% in gene expression.

The extent of *AXIN* knock-down via three different siRNAs used in the follow-up analysis was quantified, all of which revealed nearly equal inhibitions of *AXIN* expression (Figure 12).

Overall, the results suggest that *AXIN, GSK3β* and *β-catenin* are knocked-down via their specific siRNAs (Figure 10), and that the depletion of *GSK3β* and *β-catenin* seem to have a significant impact on glucose-stimulated secretion (Figure 9A). Depending on these initial findings, we proposed that glucose-stimulated secretion is regulated by Wnt target gene synthesis, in which stabilized *β-catenin* activates the synthesis of these genes leading to inhibited beta-cell secretion, in contrast to enhanced secretion upon its depletion that inactivates the transcription of Wnt target genes (Figure 3).

DISCUSSION

The main objective of my study is to find genes playing roles in pancreatic beta-cell secretory function. In this respect, a surrogate assay has been developed, where INS1-E rat pancreatic beta-cells were transfected with the SAP vector in order to estimate insulin content in the cells' media, following glucose-induced secretion. The SAP vector encodes the secreted alkaline phosphatase (SEAP) gene and thus its delivery into the beta-cells result in the localization of this vector to the secretory vesicles. Therefore, upon glucose stimulation and PMA potentiation, SAP activity detected by its substrate in beta-cells' media was shown to parallel insulin secretion (Figure 5). As indicated in the results, since this assay specifically estimates insulin release from the transfected cells, the effect of siRNA-mediated gene silencing on glucose-stimulated secretion can be detected without being masked by the cells that did not receive the siRNA agents. In this respect, the surrogate assay is a valuable tool in correlating specific genes' impact on beta-cell secretion. Additionally, the surrogate assay exhibits the desirable characteristics of high-throughput cell-based assays described as having low background noise, high reproducibility, and high signal-to-noise ratio (Cullen and Arndt, 2005). Each of these traits can be observed within the surrogate assays as low SAP activity in the untransfected cells, tight error bars for nearly all samples, and the SAP activity ratios of high glucose control to the untransfected cells, respectively. In each assay, high glucose controls have been over-sampled to enhance statistical analysis, where these controls were randomly distributed across the 96-well plate to prevent systematic errors. Thus, the surrogate assay for pancreatic beta-cell insulin secretion has been the choice of insulin secretion estimation over the direct measures of insulin content that can be obtained from

Enzyme-Linked Immunosorbent Assays (ELISA), due to the fact that these assays are less robust and more expensive.

The surrogate assay helps determine genes essential in the beta-cell secretion through siRNA-mediated gene silencing. As described in detail, the introduction of siRNAs into mammalian cells can induce unintended gene modulations, against which precautions can be taken at the state of siRNA design, as outlined in the methods section. However, since we are working with rat cells, some of these precautions may not be adequate due to incomplete resources, because all splice variants and the SNPs in the rat genes have not been predicted. Therefore, by design, we are limited to the available databases and hence additional controls within the surrogate assays become a requirement. In line with this, our follow-up screens involved the knock-down of the same gene by non-overlapping siRNAs with the aim of obtaining similar effectiveness in beta-cell secretion which, if observed, would have enhanced the confidence in the interpretation of the results. However, in our follow-up screens, the additional siRNAs targeting the same gene did not reveal similar functional consequences to the ones observed in the initial screens (Figures 8 and 11A). Several reasons that might account for such results include the differences in the efficiencies of siRNA transfections, as well as variant specificities of different siRNAs in knocking-down gene expressions. In an attempt to direct these issues, ntRFP vector has been included in the transfection components as a marker for transfection efficiency, whereas qRT-PCR analysis was performed to determine the effectiveness of specific siRNAs in the intended gene silencing.

The transfection efficiency in our screens is determined through assessing the intensity from the ntRFP vector that colocalizes to the transfected cells' nuclei. However, it should be noted that by experimental design, the transfections in our assays are underestimated since the ntRFP vector accounts for $1/4^{th}$ of the total DNA content of the transfection components, as stated in the methods. Thus, transfection efficiency determined through imaging is not a direct reflection of the components delivered into the cells. Additionally, among the transfection components of our assays, siRNAs are smaller molecules than both the SAP and ntRFP vectors, which would enable easier delivery of these molecules into the cells. Therefore, in order to have a true reflection of siRNA delivery into the cells, fluorescently labeled scrambled siRNAs can be used in the future. Scrambled siRNAs do not target any transcripts expressed in the sample by design and thus would also provide an additional level of control for the off-target effects of siRNAs exerted by sequence-independent mechanisms (Echeverri et al., 2006).

The delivery of synthetic siRNAs into mammalian cells can affect transfection efficiency, cell viability and protein expression. In order to rule out adverse effects that might be induced upon siRNA introduction into INS1-E cells, image analysis became an essential part of our screening experiments. In this respect, transmitted images of each well enabled us to visualize potential cell death or contamination within the assays. Image analysis added confidence to our secretion results through determining cell number and transfection efficiency for each well. For instance, the image data has helped us eliminate the wells with aberrantly low SAP activities that resulted from either abnormally low cell number or transfection efficiency, which were easily detected with Hoechst and Alexa 594 measurements, respectively. In addition, the determined cell

number for each sample was not only used in normalizing the secretion data, but has guided us in validating the transfection efficiency results to determine whether or not a significant difference in efficiency relates to a significantly high or low population of cells. In accordance with these aims, two rounds of raw data elimination were performed on the raw image data: the first one occurred at the level of individual assays, followed by elimination of outliers in the pooled data composed of these assays, where the details in determining the outliers are stated in the methods section. In line with this, our assays were composed of different image data including wells captured with montages of 4x4, 3x3, 2x2 or with an offset of 250. In the montages, the center of the wells are captured and enlarged for visualization purposes, whereas the images taken with an offset value captured off centered spots in the wells. Thus, the images we had for each well were restricted to specific spots on the wells. Therefore, in order to increase confidence in data analysis, the wells can be captured with offset values set to scan at least 4 different spots on the wells in order to obtain a general idea about the cells' conditions within the wells. In this way, aberrant Hoechst or Alexa 594 measurements obtained due to positional problems can be discarded from the average of these image analyses, where the problems can include low cell number due to handling during the secretion assay or simply bright spots caused by noncellular stains. On the other hand, the second round of data elimination was required on the pooled data that revealed high z-scores due to the fact that wells within each assay was pooled restricted to certain spots and hence positional problems induced outliers in the overall data points.

Image analysis has added an additional control mechanism to the interpretation of the secretion results. An example is the follow-up screen of the *FZD4* gene, which is the

strongest hit obtained from the initial screen of the IRASFS genes (Figure 6A). In the first step of the follow-up analysis, *FZD4* was knocked-down with the same siRNA that was used in the initial screen, where image data was used to normalize SAP activity to the cell number. This actually revised our view of the gene's impact on secretion, in which *FZD4* still significantly inhibited glucose-stimulated secretion, but to a lesser extent than that observed in the initial screen as depicted by the bar graphs and the F ratios (Figures 7 and 6, respectively). This difference might be a result of varying cell number within the assays, which was not taken into account in the initial screens due to lack of imaging data. In addition, a significant decrease in transfection efficiency was observed in the follow-up sample, which might explain the low SAP activity obtained in the knock-down sample (Figure 7). In contrast, the next follow-up screen performed with an additional siRNA targeting *FZD4* gene revealed that silencing this gene does not inhibit glucose-stimulated secretion and that neither the cell number nor the transfection efficiency of the sample deviated significantly from their corresponding high glucose controls (Figure 8). In the follow-up experiments for *FZD4* gene, cell number does not seem to be the factor influencing the transfection efficiencies determined (Figures 7 and 8). However, it should be pointed out that the transfection efficiency is underestimated in our assays and its determination occurs through the intensity of ntRFP vector that does not necessarily reflect siRNA delivery. Thus, transfection efficiency should be considered as an estimation of transfection in the assays. It is for this reason and the unintended gene modulations that can be induced by siRNA introduction into the mammalian cells that the gene knock-downs should be confirmed on the hits obtained from the screens. In this respect, qRT-PCR will have to be performed as a part of future follow-up studies to

confirm the knock-down of *FZD4* gene with either or both of the siRNAs of interest, in order to assign a role for this gene in the beta-cell function.

In the case of the initial screen performed on the Wnt signaling pathway components, the knock-down of *AXIN*, *GSK3β* and *β-catenin* genes was confirmed through qRT-PCR analysis (Figure 10) and that the depletion of *AXIN* and *GSK3β* resulted in inhibited secretion, whereas silencing *β-catenin* was shown to enhance glucose-induced secretion (Figure 9A). In the image analysis, significant inhibition in transfection efficiencies corresponded to each hit (Figure 9B). Since glucose-stimulated secretion is a reflection of secreted SAP activity in the media, inhibited secretion can be correlated to low transfection efficiency. However, this assumption does not hold true for *β-catenin* silenced samples, where enhanced SAP activity corresponds to inhibited transfection efficiency. Therefore, as pointed out previously, the transfection efficiency should be considered as an estimate of transfection, rather than a direct correlation to measured SAP activity in the cells' media, where it is likely that underestimation of the transfection efficiency might induce the variation observed. For that reason, follow-up analyses are crucial. *AXIN* gene was the focus of our studies and this gene was knocked-down with two additional siRNAs to compare the effects in secretion to the one observed by initial siRNA knock-down (Figure 11). From these analyses, it can be deduced that only the initial siRNA caused a significant inhibition of glucose-induced secretion, where the additional siRNAs did not impede secretion (Figure 11A). Surprisingly, qRT-PCR results revealed that all the siRNAs are equally capable of *AXIN* gene silencing in INS1-E cells (Figure 12), which raised the question of why a consistent effect on secretion was not observed. One way to address this question is to perform rat insulin ELISA on the

insulin secreted media to obtain a direct measure of insulin release that would add confidence into the SAP results. This validation becomes essential when the transfection efficiency for the knock-downs parallel SAP activity is considered (Figure 11A and B). On the other hand, another possible explanation for the contradictory secretion results could be the siRNA targets themselves, where the off-targeted gene silencing was attributed to the sequence similarity between an siRNA duplex and a non-targeted mRNA molecule in the seed region composed of 7 nucleotides on the 5' region of the siRNA guide strand (Jackson et al., 2006). In this respect, the siRNAs used to knock-down the *AXIN* gene were blasted against the rat genome that revealed the following mismatches with similar genes in the rat genome: 4 mismatches at the 5'end, 4 mismatches at the 3'end and 3 mismatches at the 3' end of the siRNA guide strands for the siRNAs used in AXIN#1, AXIN#2 and AXIN#3 samples, respectively (Figure 12). It can be hypothesized that the inconsistency in secretion from the different knock-downs might be a result of off-targeted gene silencing, which has a higher probability of occurrence in the sample AXIN#1 due to the fact that the mismatch with the next similar gene *Wee 1* resides in the seed region of the siRNA used in this sample. This assumption is actually supported by the secretion results observed from the *AXIN* knock-downs with two additional siRNAs that did not effect secretion (Figure 11). However, there is no report that suggests a role for the *Wee1* gene in pancreatic beta-cell function. This gene plays a crucial role in the pre-implantation stages of mouse embryonic development (Tominaga et al., 2006), in addition to its defined function as a coordinator of the transition between DNA replication and mitosis. The lack of evidence for *Wee1* involvement in beta-cell function comes from the limited number of studies performed on this gene. However, since it is

involved in the regulation of the cell cycle, it might be an important gene for pancreatic development. Therefore, it might be worthwhile to quantify its knock-down in siAXIN#1 samples in order to be precise about the conclusion drawn from the *AXIN* follow-up analyses. However, based on our analyses on the Wnt signaling pathway components, *AXIN* does not appear to be a true hit, whereas *GSK3β* and *β-catenin* are promising hits, whose effects on glucose-induced secretion need to be further validated through follow-up screens with additional siRNAs with a confirmed knock-down of these genes through qRT-PCR analyses.

For all the hits obtained from the screens, qRT-PCR has been the initial step in confirming the gene knock-down, which validated the effect observed in secretion. However, in order to assign a role for each hit in the beta-cell function, the protein depletion should also be confirmed through either Western Blot analysis or immunofluorescence, which are included within the future directions of this project.

Reference List

Allgot B., Gan D., King H., Lefebvre P., Mbanya J., Silink M., Siminerio L., Williams R., Zimmet P., and Regniers C. Diabetes Atlas [Second Edition]. 2003. International Diabetes Federation.
Ref Type: Magazine Article

Almasy,L. and Blangero,J. (1998). Multipoint quantitative-trait linkage analysis in general pedigrees. Am. J. Hum. Genet. *62*, 1198-1211.

Antinozzi,P.A., Ishihara,H., Newgard,C.B., and Wollheim,C.B. (2002). Mitochondrial metabolism sets the maximal limit of fuel-stimulated insulin secretion in a model pancreatic beta cell: a survey of four fuel secretagogues. J. Biol. Chem. *277*, 11746-11755.

Ashcroft,F.M. (2006). K(ATP) channels and insulin secretion: a key role in health and disease. Biochem. Soc. Trans. *34*, 243-246.

Barg,S., Eliasson,L., Renstrom,E., and Rorsman,P. (2002). A subset of 50 secretory granules in close contact with L-type Ca2+ channels accounts for first-phase insulin secretion in mouse beta-cells. Diabetes *51 Suppl 1*, S74-S82.

Bergman,R.N., Ader,M., Huecking,K., and Van,C.G. (2002). Accurate assessment of beta-cell function: the hyperbolic correction. Diabetes *51 Suppl 1*, S212-S220.

Birmingham,A., Anderson,E., Sullivan,K., Reynolds,A., Boese,Q., Leake,D., Karpilow,J., and Khvorova,A. (2007). A protocol for designing siRNAs with high functionality and specificity. Nat. Protoc. *2*, 2068-2078.

Blumenthal,A., Ehlers,S., Lauber,J., Buer,J., Lange,C., Goldmann,T., Heine,H., Brandt,E., and Reiling,N. (2006). The Wingless homolog WNT5A and its receptor Frizzled-5 regulate inflammatory responses of human mononuclear cells induced by microbial stimulation. Blood *108*, 965-973.

Cadigan,K.M. and Liu,Y.I. (2006). Wnt signaling: complexity at the surface. J. Cell Sci. *119*, 395-402.

Catterall,W.A. (1999). Interactions of presynaptic Ca2+ channels and snare proteins in neurotransmitter release. Ann. N. Y. Acad. Sci. *868*, 144-159.

Cauchi,S., El,A.Y., Choquet,H., Dina,C., Krempler,F., Weitgasser,R., Nejjari,C., Patsch,W., Chikri,M., Meyre,D., and Froguel,P. (2007). TCF7L2 is reproducibly associated with type 2 diabetes in various ethnic groups: a global meta-analysis. J. Mol. Med. *85*, 777-782.

Cullen,L.M. and Arndt,G.M. (2005). Genome-wide screening for gene function using RNAi in mammalian cells. Immunol. Cell Biol. *83*, 217-223.

Daniels,D.L. and Weis,W.I. (2005). Beta-catenin directly displaces Groucho/TLE repressors from Tcf/Lef in Wnt-mediated transcription activation. Nat. Struct. Mol. Biol. *12*, 364-371.

DasGupta,R., Kaykas,A., Moon,R.T., and Perrimon,N. (2005). Functional genomic analysis of the Wnt-wingless signaling pathway. Science *308*, 826-833.

Dodson,G. and Steiner,D. (1998). The role of assembly in insulin's biosynthesis. Curr. Opin. Struct. Biol. *8*, 189-194.

Dudbridge,F. (2003). Pedigree disequilibrium tests for multilocus haplotypes. Genet. Epidemiol. *25*, 115-121.

Dupre,D.J. and Hebert,T.E. (2006). Biosynthesis and trafficking of seven transmembrane receptor signalling complexes. Cell Signal. *18*, 1549-1559.

Echeverri,C.J., Beachy,P.A., Baum,B., Boutros,M., Buchholz,F., Chanda,S.K., Downward,J., Ellenberg,J., Fraser,A.G., Hacohen,N., Hahn,W.C., Jackson,A.L., Kiger,A., Linsley,P.S., Lum,L., Ma,Y., Mathey-Prevot,B., Root,D.E., Sabatini,D.M., Taipale,J., Perrimon,N., and Bernards,R. (2006). Minimizing the risk of reporting false positives in large-scale RNAi screens. Nat. Methods *3*, 777-779.

Eliasson,L., Renstrom,E., Ding,W.G., Proks,P., and Rorsman,P. (1997). Rapid ATP-dependent priming of secretory granules precedes Ca(2+)-induced exocytosis in mouse pancreatic B-cells. J. Physiol *503 (Pt 2)*, 399-412.

Force,T., Woulfe,K., Koch,W.J., and Kerkela,R. (2007). Molecular scaffolds regulate bidirectional crosstalk between Wnt and classical seven-transmembrane-domain receptor signaling pathways. Sci. STKE. *2007*, e41.

Fujino,T., Asaba,H., Kang,M.J., Ikeda,Y., Sone,H., Takada,S., Kim,D.H., Ioka,R.X., Ono,M., Tomoyori,H., Okubo,M., Murase,T., Kamataki,A., Yamamoto,J., Magoori,K., Takahashi,S., Miyamoto,Y., Oishi,H., Nose,M., Okazaki,M., Usui,S., Imaizumi,K., Yanagisawa,M., Sakai,J., and Yamamoto,T.T. (2003). Low-density lipoprotein receptor-related protein 5 (LRP5) is essential for normal cholesterol metabolism and glucose-induced insulin secretion. Proc. Natl. Acad. Sci. U. S. A *100*, 229-234.

Galli,L.M., Barnes,T., Cheng,T., Acosta,L., Anglade,A., Willert,K., Nusse,R., and Burrus,L.W. (2006). Differential inhibition of Wnt-3a by Sfrp-1, Sfrp-2, and Sfrp-3. Dev. Dyn. *235*, 681-690.

Goldman,M.A. (2004). RNAi for research and therapy. Genome Biol. *5*, 342.

Gordon,M.D. and Nusse,R. (2006). Wnt signaling: multiple pathways, multiple receptors, and multiple transcription factors. J. Biol. Chem. *281*, 22429-22433.

Habas,R. and Dawid,I.B. (2005). Dishevelled and Wnt signaling: is the nucleus the final frontier? J. Biol. *4*, 2.

Hattersley,A.T. (2007). Prime suspect: the TCF7L2 gene and type 2 diabetes risk. J. Clin. Invest *117*, 2077-2079.

Heller,R.S., Dichmann,D.S., Jensen,J., Miller,C., Wong,G., Madsen,O.D., and Serup,P. (2002). Expression patterns of Wnts, Frizzleds, sFRPs, and misexpression in transgenic mice suggesting a role for Wnts in pancreas and foregut pattern formation. Dev. Dyn. *225*, 260-270.

Heller,R.S., Klein,T., Ling,Z., Heimberg,H., Katoh,M., Madsen,O.D., and Serup,P. (2003). Expression of Wnt, Frizzled, sFRP, and DKK genes in adult human pancreas. Gene Expr. *11*, 141-147.

Henkin,L., Bergman,R.N., Bowden,D.W., Ellsworth,D.L., Haffner,S.M., Langefeld,C.D., Mitchell,B.D., Norris,J.M., Rewers,M., Saad,M.F., Stamm,E., Wagenknecht,L.E., and Rich,S.S. (2003). Genetic epidemiology of insulin resistance and visceral adiposity. The IRAS Family Study design and methods. Ann. Epidemiol. *13*, 211-217.

Henquin,J.C. (2000). Triggering and amplifying pathways of regulation of insulin secretion by glucose. Diabetes *49*, 1751-1760.

Hermann,M., Pirkebner,D., Draxl,A., Berger,P., Untergasser,G., Margreiter,R., and Hengster,P. (2007). Dickkopf-3 is expressed in a subset of adult human pancreatic beta cells. Histochem. Cell Biol. *127*, 513-521.

Holmen,S.L., Salic,A., Zylstra,C.R., Kirschner,M.W., and Williams,B.O. (2002). A novel set of Wnt-Frizzled fusion proteins identifies receptor components that activate beta -catenin-dependent signaling. J. Biol. Chem. *277*, 34727-34735.

Huang,H.C. and Klein,P.S. (2004). The Frizzled family: receptors for multiple signal transduction pathways. Genome Biol. *5*, 234.

Inaki,M., Yoshikawa,S., Thomas,J.B., Aburatani,H., and Nose,A. (2007). Wnt4 is a local repulsive cue that determines synaptic target specificity. Curr. Biol. *17*, 1574-1579.

Jackson,A.L., Bartz,S.R., Schelter,J., Kobayashi,S.V., Burchard,J., Mao,M., Li,B., Cavet,G., and Linsley,P.S. (2003). Expression profiling reveals off-target gene regulation by RNAi. Nat. Biotechnol. *21*, 635-637.

Jackson,A.L., Burchard,J., Schelter,J., Chau,B.N., Cleary,M., Lim,L., and Linsley,P.S. (2006). Widespread siRNA "off-target" transcript silencing mediated by seed region sequence complementarity. RNA. *12*, 1179-1187.

Jin,T. (2008). The WNT signalling pathway and diabetes mellitus. Diabetologia *51*, 1771-1780.

Kanazawa,A., Tsukada,S., Sekine,A., Tsunoda,T., Takahashi,A., Kashiwagi,A., Tanaka,Y., Babazono,T., Matsuda,M., Kaku,K., Iwamoto,Y., Kawamori,R., Kikkawa,R., Nakamura,Y., and Maeda,S. (2004). Association of the gene encoding wingless-type

mammary tumor virus integration-site family member 5B (WNT5B) with type 2 diabetes. Am. J. Hum. Genet. *75*, 832-843.

Kasuga,M. (2006). Insulin resistance and pancreatic beta cell failure. J. Clin. Invest *116*, 1756-1760.

Kikuchi,A. and Yamamoto,H. (2008). Tumor formation due to abnormalities in the beta-catenin-independent pathway of Wnt signaling. Cancer Sci. *99*, 202-208.

Kikuchi,A., Yamamoto,H., and Kishida,S. (2007). Multiplicity of the interactions of Wnt proteins and their receptors. Cell Signal. *19*, 659-671.

Kim,H.J., Schleiffarth,J.R., Jessurun,J., Sumanas,S., Petryk,A., Lin,S., and Ekker,S.C. (2005). Wnt5 signaling in vertebrate pancreas development. BMC. Biol. *3*, 23.

Kohn,A.D. and Moon,R.T. (2005). Wnt and calcium signaling: beta-catenin-independent pathways. Cell Calcium *38*, 439-446.

Krupnik,V.E., Sharp,J.D., Jiang,C., Robison,K., Chickering,T.W., Amaravadi,L., Brown,D.E., Guyot,D., Mays,G., Leiby,K., Chang,B., Duong,T., Goodearl,A.D., Gearing,D.P., Sokol,S.Y., and McCarthy,S.A. (1999). Functional and structural diversity of the human Dickkopf gene family. Gene *238*, 301-313.

Kuhl,M., Sheldahl,L.C., Park,M., Miller,J.R., and Moon,R.T. (2000). The Wnt/Ca2+ pathway: a new vertebrate Wnt signaling pathway takes shape. Trends Genet. *16*, 279-283.

Lyssenko,V., Lupi,R., Marchetti,P., Del,G.S., Orho-Melander,M., Almgren,P., Sjogren,M., Ling,C., Eriksson,K.F., Lethagen,A.L., Mancarella,R., Berglund,G., Tuomi,T., Nilsson,P., Del,P.S., and Groop,L. (2007). Mechanisms by which common variants in the TCF7L2 gene increase risk of type 2 diabetes. J. Clin. Invest *117*, 2155-2163.

MacDonald,P.E., Joseph,J.W., and Rorsman,P. (2005). Glucose-sensing mechanisms in pancreatic beta-cells. Philos. Trans. R. Soc. Lond B Biol. Sci. *360*, 2211-2225.

MacDonald,P.E. and Rorsman,P. (2007). The ins and outs of secretion from pancreatic beta-cells: control of single-vesicle exo- and endocytosis. Physiology. (Bethesda.) *22*, 113-121.

Masharani U. and German M.S. (2007). Pancreatic Hormones & Diabetes Mellitus. In Greenspan's Basic and Clinical Endocrinology, The McGraw-Hill Companies, Inc.).

Meetoo,D., McGovern,P., and Safadi,R. (2007). An epidemiological overview of diabetes across the world. Br. J. Nurs. *16*, 1002-1007.

Mendez,C.F., Leibiger,I.B., Leibiger,B., Hoy,M., Gromada,J., Berggren,P.O., and Bertorello,A.M. (2003). Rapid association of protein kinase C-epsilon with insulin granules is essential for insulin exocytosis. J. Biol. Chem. *278*, 44753-44757.

Molenaar,M. and Destree,O. (1999). A tight control over Wnt action. Int. J. Dev. Biol. *43*, 675-680.

Molina P.E. (2006). Endocrine Pancreas. In Endocrine Physiology, The McGraw-Hill Companies, Inc.).

Muoio,D.M. and Newgard,C.B. (2008). Mechanisms of disease: molecular and metabolic mechanisms of insulin resistance and beta-cell failure in type 2 diabetes. Nat. Rev. Mol. Cell Biol. *9*, 193-205.

Nelson D.L.and Cox M.M. (2005). Principles of Biochemistry. W. H. Freeman and Company).

Newgard,C.B. and McGarry,J.D. (1995). Metabolic coupling factors in pancreatic beta-cell signal transduction. Annu. Rev. Biochem. *64*, 689-719.

Newsholme,P., Bender,K., Kiely,A., and Brennan,L. (2007). Amino acid metabolism, insulin secretion and diabetes. Biochem. Soc. Trans. *35*, 1180-1186.

Palmer,N.D., Langefeld,C.D., Campbell,J.K., Williams,A.H., Saad,M., Norris,J.M., Haffner,S.M., Rotter,J.I., Wagenknecht,L.E., Bergman,R.N., Rich,S.S., and Bowden,D.W. (2006). Genetic mapping of disposition index and acute insulin response loci on chromosome 11q. The Insulin Resistance Atherosclerosis Study (IRAS) Family Study. Diabetes *55*, 911-918.

Palmer,N.D., Lehtinen,A.B., Langefeld,C.D., Campbell,J.K., Haffner,S.M., Norris,J.M., Bergman,R.N., Goodarzi,M.O., Rotter,J.I., and Bowden,D.W. (2008). Association of TCF7L2 gene polymorphisms with reduced acute insulin response in Hispanic Americans. J. Clin. Endocrinol. Metab *93*, 304-309.

Pereira,C., Schaer,D.J., Bachli,E.B., Kurrer,M.O., and Schoedon,G. (2008). Wnt5A/CaMKII signaling contributes to the inflammatory response of macrophages and is a target for the antiinflammatory action of activated protein C and interleukin-10. Arterioscler. Thromb. Vasc. Biol. *28*, 504-510.

Prentki,M. and Nolan,C.J. (2006). Islet beta cell failure in type 2 diabetes. J. Clin. Invest *116*, 1802-1812.

Reynolds,A., Anderson,E.M., Vermeulen,A., Fedorov,Y., Robinson,K., Leake,D., Karpilow,J., Marshall,W.S., and Khvorova,A. (2006). Induction of the interferon response by siRNA is cell type- and duplex length-dependent. RNA. *12*, 988-993.

Rorsman,P., Eliasson,L., Renstrom,E., Gromada,J., Barg,S., and Gopel,S. (2000). The Cell Physiology of Biphasic Insulin Secretion. News Physiol Sci. *15*, 72-77.

Rutter,G.A., Tsuboi,T., and Ravier,M.A. (2006). Ca2+ microdomains and the control of insulin secretion. Cell Calcium *40*, 539-551.

Schinner,S., Ulgen,F., Papewalis,C., Schott,M., Woelk,A., Vidal-Puig,A., and Scherbaum,W.A. (2008). Regulation of insulin secretion, glucokinase gene transcription and beta cell proliferation by adipocyte-derived Wnt signalling molecules. Diabetologia *51*, 147-154.

Shu,L., Sauter,N.S., Schulthess,F.T., Matveyenko,A.V., Oberholzer,J., and Maedler,K. (2008). Transcription factor 7-like 2 regulates beta-cell survival and function in human pancreatic islets. Diabetes *57*, 645-653.

Smith,U. (2007). TCF7L2 and type 2 diabetes--we WNT to know. Diabetologia *50*, 5-7.

Takada,R., Hijikata,H., Kondoh,H., and Takada,S. (2005). Analysis of combinatorial effects of Wnts and Frizzleds on beta-catenin/armadillo stabilization and Dishevelled phosphorylation. Genes Cells *10*, 919-928.

Tominaga,Y., Li,C., Wang,R.H., and Deng,C.X. (2006). Murine Wee1 plays a critical role in cell cycle regulation and pre-implantation stages of embryonic development. Int. J. Biol. Sci. *2*, 161-170.

Varadi,A., Ainscow,E.K., Allan,V.J., and Rutter,G.A. (2002). Involvement of conventional kinesin in glucose-stimulated secretory granule movements and exocytosis in clonal pancreatic beta-cells. J. Cell Sci. *115*, 4177-4189.

Wang,Z., Shu,W., Lu,M.M., and Morrisey,E.E. (2005). Wnt7b activates canonical signaling in epithelial and vascular smooth muscle cells through interactions with Fzd1, Fzd10, and LRP5. Mol. Cell Biol. *25*, 5022-5030.

WHO. World Health Organization Fact Sheet Diabetes. 2006. WHO Press Office. Ref Type: Report

Wiederkehr,A. and Wollheim,C.B. (2006). Minireview: implication of mitochondria in insulin secretion and action. Endocrinology *147*, 2643-2649.

Yamamoto,H., Komekado,H., and Kikuchi,A. (2006). Caveolin is necessary for Wnt-3a-dependent internalization of LRP6 and accumulation of beta-catenin. Dev. Cell *11*, 213-223.

Zaitsev,S.V., Efendic,S., Arkhammar,P., Bertorello,A.M., and Berggren,P.O. (1995). Dissociation between changes in cytoplasmic free Ca2+ concentration and insulin secretion as evidenced from measurements in mouse single pancreatic islets. Proc. Natl. Acad. Sci. U. S. A *92*, 9712-9716.

Zuhorn,I.S., Engberts,J.B., and Hoekstra,D. (2007). Gene delivery by cationic lipid vectors: overcoming cellular barriers. Eur. Biophys. J. *36*, 349-362.

APPENDIX

Table 1. Ligand and receptor couplings in the Wnt signaling pathway.

Ligand	Receptor	organism/ cell line	Function	Reference
Wnt5a	Fzd5	*Drosophila*	Activates β-catenin pathway	Kikuchi et al., 2007
Wnt5a	Fzd4-LRP5	*Drosophila*	Activates β-catenin pathway	Kikuchi et al., 2007
Wnt5a	Fzd4	Mammals	Activates PKC (Wnt/Ca^{2+} pathway), Fzd4 internalized	Kikuchi et al., 2007
Wnt5a	Fzd5	Mammals	Fzd5 internalized without PKC activation	Kikuchi et al., 2007
Wnt3a	Fzd5	Mammals	Fzd5 internalized	Kikuchi et al., 2007
Wnt1 or Wnt3a	LRP6	Mouse	Activates β-catenin pathway	Holmen et al., 2002
Wnt8	LRP6	*Xenopus*	Activates β-catenin pathway	Holmen et al., 2002
XWnt8-hFzd5 construct	LRP6	293T cell	Activates β-catenin pathway	Holmen et al., 2002
XWnt11-hFzd5 construct	LRP6	293T cell	Activates β-catenin pathway	Holmen et al., 2002
XWnt5a-hFzd5 construct	LRP6	293T cell	Activates β-catenin pathway	Holmen et al., 2002
Wnt5a	Fzd5	Human macrophages	Activates CamKII; APC interferes with Wnt5a signaling	Pereira et al., 2008
Wnt5a	Fzd5	Human macrophages	Regulation of the response to microbial stimulation	Blumenthal et al., 2006
Wnt4	Fzd2	*Drosophila*	Determines synaptic target specificity	Inaki et al., 2007
Wnt3a	-	HEK293 cells	Activates β-catenin pathway	Yamamoto et al., 2006
Wnt5a	Fzd5-LRP6	-	Activates β-catenin pathway; Fzd5 is internalized	Yamamoto et al., 2006
Dkk1	LRP6	-	Activates β-catenin pathway in the absence of Wnt stimulation	Cadigan and Liu, 2006
Wnt5a	Fzd1-10	HEK293	Incapable of activation β-catenin pathway	Cadigan and Liu, 2006
Wnt3a	sFRP1 & 2	L cells	Inhibits Wnt3a induced β-catenin accumulation	Galli et al., 2006
Wnt3a	Fzd 4, 5 and 8	*Drosophila*	Activates β-catenin pathway	Takada et al., 2005
Wnt7b	Fzd1 & 10 and LRP5	Mouse embryonic lung sections	Activates β-catenin pathway; induces lung development	Wang et al., 2005
Wnt5	Fzd2	Mouse	Involved in islet formation	Heller et al., 2002
Wnt5	Fzd2	Zebrafish	Insulin cell migration in islet formation	Kim et al., 2005
Wnt5a	rFzd2	Zebrafish	Wnt/Ca^{2+} pathway activation	Kuhl et al., 2000
Wnt8	rFzd1	-	Activates β-catenin pathway	Kuhl et al., 2000

Fzd: Frizzled, LRP: Low-density lipoprotein related protein, XWnt: *Xenopus* Wnt, hFzd: human Frizzled, Dkk1: Dickkopf 1, sFRP1: secreted Frizzled related protein, rFzd: rat Frizzled

Table 2. Prioritization scheme and number of loci based on detailed molecular genetic analysis of chromosome 11.

Priority	Trait	Test	Location	P-value for Association	# of Independent Loci	Cumulative number of Loci	Gene(s)
1	AIR **and** DI	QPDT **and** SOLAR	Gene	<0.01	1	1	*GAB2*
2	AIR **and** DI	QPDT **and** SOLAR	Gene	<0.05	0	1	-
3	AIR **and/or** DI	QPDT **or/and** SOLAR	Gene	<0.001	1	2	*MRPL48*
4	AIR **and/or** DI	QPDT **or/and** SOLAR	Gene	<0.01	7	9	*ME3,UVRAG, PGM2L1, CCDC83, DLG2*
5	AIR **and/or** DI	QPDT **or/and** SOLAR	Gene	<0.05	8	17	*RPS3,C11orf30, PCF11,KCNE3*
6	AIR **or** DI	QPDT **or** SOLAR	Gene	<0.001	1	18	
7	AIR **or** DI	QPDT **or** SOLAR	Gene	<0.01	1	19	*WNT11*
8	AIR **or** DI	QPDT **or** SOLAR	Gene	<0.05	30	49	*MAP6, SLCO2B1, HBXAP, SERPINH1, FZD4 LRRC32, RAB30, EED, SYTL2, PAK1*

Table 3. The complete list of IRASFS genes and their functions.

SYMBOL	NAME	DESCRIPTION
FZD4	frizzled homolog 4	Positive regulator of the Wingless type MMTV integration site signaling pathway
RPS3	ribosomal protein S3	A ribosomal protein that is a component of the 40S subunit
PAK1	p21/Cdc42/Rac1-activated kinase1 (STE homolog, yeast)	Regulates cell motility and morphology
PGM2L1	phosphoglucomutase 2-like 1	-
PCF11	cleavage and polyadenylation factor subunit	-
MRPL48	mitochondrial ribosomal protein L48	Encodes the mammalian mitochondrial ribosomal 39S subunit
UVRAG	UV radiation resistance associated gene	complements UV sensitivity of xeroderma pigmentosum group C cells; suppresses tumorigenicity of human colon cancer cells
WNT11	wingless-type MMTV integration site family, member 11	May play a role in the development of skeleton, kidney and lung
RAB30	RAB30, member RAS oncogene family	-
ME3	malic enzyme 3, $NADP^+$-dependent, mitochondrial	Catalyzes the oxidative decarboxylation of malate to pyruvate
UCP3	uncoupling protein 3 (mitochondrial, proton carrier)	Separate oxidative phosphorylation from ATP synthesis with energy dissipated as heat
PC	pyruvate carboxylase	Involved in gluconeogenesis, lipogenesis, insulin secretion and synthesis of the neurotransmitter glutamate
GAB2	GRB2-associated binding protein 2	Principal activator of phosphatidylinositol-3 kinase in response to activation of the high affinity IgE receptor
SLCO2B1	solute carrier organic anion transporter family, member 2B1	-
SERPINH1	serpin peptidase inhibitor, clade H, member 1	Localizes to the ER lumen and binds collagen; could be involved in the maturation of collagen molecules
LRRC32	leucine rich repeat containing 32	Type 1 membrane protein which contains 20 leucine rich repeats
DLG2	discs, large homolog 2, chapsyn-110	A member of the membrane-associated guanylate kinase (MAGUK) family
KCNE3	potassium voltage-gated channel, Isk-related family, member 3	Modulates the gating kinetics and enhance stability of the multimeric complex
HBXAP	hepatitis B virus x associated protein	Involved in transcription repression, transcription coactivation, and chromatin remodeling and spacing
SYTL2	synaptotagmin-like 2	Shown to bind the GTP-bound form of Ras-related protein Rab-27A (RAB27A), suggesting a role in vesicle trafficking
MAP6	microtubule-associated protein 6	Calmodulin-binding and calmodulin-regulated protein that is involved in microtubule stabilization
C11orf30	chromosome 11 open reading frame 30	Hypothetical protein
EED	embryonic ectoderm development	Mediates repression of gene activity through histone deacetylation and may act as a regulator of integrin function
CCDC83	Coiled-coil domain containing 83	Hypothetical protein

SCHOLASTIC VITA

FEYZA NUR TUNCER

ADDRESS:

BUSINESS: Wake Forest University Graduate School
of Arts and Sciences
Molecular Genetics Program
Medical Center Boulevard
Winston-Salem, NC 27157

PERSONAL INFORMATION:

BIRTHPLACE: Istanbul, Turkey

BIRTH DATE: January 19, 1984

CITIZENSHIP: Turkey

EDUCATION:

2006-PRESENT: Wake Forest University Graduate School
of Arts and Sciences
Winston-Salem, NC
Master of Science December 2008

2002-2006: Sabanci University (SU)
Istanbul, Turkey
B.S., Biological Sciences and Bioengineering

PROFESSIONAL EXPERIENCE:

2005-2006: ENS 491/492 Graduation Project, Dr. Zehra Sayers, Ph.D. and Dr. Suzanne Hart, PhD., collaboration between Sabanci University (SU) and National Human Genome Research Institute, SU Biological Research Laboratory, Istanbul, Turkey

2005: Proj 301, Summer Student, Dr. Suzanne Hart, Ph.D., National Human Genome Research Institute, National Institutes of Health, Bethesda, USA

2004: Intern, Prof. Dr. Osman Muftuoglu, M.D., Yasasin Hayat Clinic, Istanbul, Turkey

2003:	Intern, Dr. Julide Caferler, M.D., and Dr. Hakan Ozon, M.D., Genetic Research Center Laboratory, Deutsches Krankenhaus Universal Hospitals Group, Istanbul, Turkey
2002:	Intern, Canan Sarpel, M.S., Microbiology Laboratory, International Hospital, Istanbul, Turkey

TEACHING EXPERIENCE:

2007-PRESENT:	Brain Awareness Council Volunteer Chair, volunteering and organizing visits to local elementary, middle and high schools to teach about brain and science, Winston-Salem, NC, USA
2005:	Teaching Assistant, Dr. Hikmet Budak, Ph.D., PROJ 102 on Genetically Modified Organisms (GMO) for Sabanci University's freshmen students, Istanbul, Turkey
2005:	Laboratory Assistant, Dr. Selim Çetiner, Ph.D., teaching basic laboratory skills to Sabanci University's sophomore students, Istanbul, Turkey

CONFERENCES and WORKSHOPS:

2007:	Poster competition finalist, "Development of a high-throughput screen to validate candidate disease susceptibility genes", Charlotte Biotechnology Conference, University of North Carolina Charlotte (UNCC), NC, USA
2004:	Volunteer, "Maternal and Child Health"; governmental project on the emphasis of breast feeding, Health Management of Istanbul, Turkey
2004:	Organization Committee Member, National Symposium: Agricultural Biotechnology in Turkey, Sabanci University, Istanbul, Turkey

CIVIC INVOLVEMENT PROJECTS (CIPs):

2004-2006:	Project Assistant: Coordinating two projects, Bahcelievler Orphanage (children ages 0-6 yrs old) and Sultanbeyli Elementary School (children ages 7-12 yrs old), Istanbul, Turkey
2003-2004:	Supervisor: Coordinating a team of 20 students at Sabanci University to assist the academic and social development of orphan teenagers
2003:	Organizer & Participant, Fourth International Volunteer Summer Work Camp at Sabanci University Campus*:* organizing activities to international volunteers. Summer camp organization for economically underdeveloped families' children, Istanbul, Turkey
2002-2003:	Volunteer: teaching various subjects and organizing social activities for educational and social development of children at Ballica Elementary School, Istanbul, Turkey